이학석사 학위논문

Combined Proteomics and Metabolomics Study Reveals the TNF-α Regulated Metabolic Reprogramming of Estrogen Receptor/Progesterone Receptor Positive and Triple Negative Breast Cancer Cells

오믹스 분석을 통한 TNF-α에 의해 조절되는 음성/양성 유방암 세포주의 미토콘드리아 대사 리프로그래밍 기전 규명

2020 년 02 월

서울대학교 대학원

분자의학 및 바이오제약학과

이 하 연

Abstract

Combined Proteomics and Metabolomics Study Reveals the TNF-α Regulated Metabolic Reprogramming of Estrogen Receptor/Progesterone Receptor Positive and Triple Negative Breast Cancer Cells

Ha Yun Lee
Molecular Medicine and Biopharmaceutical Sciences
Graduate School of Convergence Science and Technology
Seoul National University

The Warburg effect has long been considered as the metabolic process in cancer cells, however, now it has been revealed that the metabolism process differs according to types of cancers. Among the cell organelles, the mitochondrion not only modulates ATP production but also the oncogenesis by generating building blocks for tumor anabolism, controlling redox and metastasis. Here, we investigated the metabolism change of mitochondria in two different breast cancer cell lines, ER/PR receptor□positive and triple negative, inducing the reprogramming by tumor necrosis factor-α (TNF-α). TNF-α is cytokine that increases in level at the very initial stage of the tumor microenvironment and is known to play dual role in onco-immunology either acting

as an anti-cancer factor or behaving as an immunosuppressive cytokine depending upon the stage and type of cancer. Using proteomics and metabolomics approach, we have investigated the metabolism reprogramming on two different breast cancer cell lines, MCF7, ER/PR positive luminal cell line, and MDA-MB231, triple negative basal-like cell line, in presence of TNF-α. The results here strongly suggest that the activation of mitochondria oxidative phosphorylation differs in two cell lines under the TNF-α treated or untreated conditions, as the electron transport chain (ETC) complex alters their assembly state. Our research revealed the association between the metabolic state and the response to cytokines in two different cell lines, which can be the basis for future of identifying targets of therapeutic response in heterogenous of breast cancer.

Keywords : Proteomics, Metabolomics, Breast Cancer Heterogeneity, TNF-α, Mitochondria
Student Number : 2018-26193

Abbreviation

ER estrogen receptor
PR progesterone receptor
TNF-α tumor necrosis factor-α
ROS reactive oxygen species
IMM inner mitochondrial membrane
FBXL4 F-box and leucine-rich repeat protein 4
OXPHOS oxidative phosphorylation
PTM post-translational modification
2DG 2-deoxy-glucose
DDA data-dependent acquisition
DEP differentially expressed protein
PLGEM-STN power law global error model-signal to noise
MAI moment adjusted imputation
IPA Ingenuity Pathway Analysis
PANTHER Protein Analysis through Evolutionary Relationships Classification System
QQQ triple-quadrupole
CE collision energy
CV coefficient of variation
TCG The Cancer Genome Atlas
ETC electron transport chain
SC super-complex
2-HG 2-hydroxyglutarate
HDM histone demethylases
Fe-S iron sulfur

Table of Contents

List of Figures

Figure 3. The level of differentially regulated metabolites under the TNF-α treated condition in MCF7 and MDA-MB231 cells. (A) Targeted metabolomics analysis of 18 metabolites (glucose-6-phosphate (G6P), ribose-5-phosphate (R5P), fructose-6-phosphate (F6P), fructose-1,6-phosphate (F1,6BP), glyceraldehyde-3-phosphate (GA3P), dihydroxyacetone phosphate, pyruvate, lactate, citrate, aconitate, iso-citrate, α-ketoglutarate, glutamate, succinate, fumarate, malate, oxaloacetate, and aspartate) related to glycolysis and TCA cycle in MCF7 and MDA-MB231 in the presence and absence of TNF-α. (B) Functional enrichment of metabolism processes and the up/down-regulation of proteins and metabolites.

Figure 4. The assembly and activation of oxidative phosphorylation under the TNF-α treated condition in MCF7 and MDA-MB231 cells. (A) Functional analysis showing ATP related functions in MCF7 and MDA-MB231. (B) MCF7 and MDA-MB231 cells were treated with TNF-α (10 ng/μl) for 24 h with or without MG132 (10 μM) for 8 h. After treatment, mitochondria fraction was isolated and further analyzed by BN-PAGE and in-gel enzyme staining as described in Methodology. (C) The biological network analysis of complex proteins of MDA-MB231 under TNF-α treatment. Associations among proteins are shown by gray lines, which represent direct or indirect interactions. Up-regulated proteins are shown in red, and down-regulated proteins are shown in blue. (D) and (E) MCF7 and MDA-MB231 cells were treated with TNF-α (10 ng/μl) and 2DG (10 mM) either alone or in combination for 24

h and complex I and complex II activity was measured spectrophotometrically.

Figure 5. The level of differentially regulated ATP. (A) and (B) MCF7 and MDA-MB231 cells were treated with TNF-α alone or in combination with 2DG (10 mM) and the steady-state ATP levels were determined by luciferase-based assay as described in Methodology. (C) and (D) MCF7 and MDA-MB231 cells were treated with TNF-α alone or in combination with 2DG (10 mM) and the mitochondria generated ATP levels were determined.

Figure 6. Differentially regulated ubiquitinated proteins. (A) The biological network analysis of DEPs. Associations among DEPs are shown by gray lines, which represent direct or indirect interactions. Up-regulated proteins are shown in red, and down-regulated proteins are shown in green. (B) Molecular functions of DEPs by IPA tool. The x-axis indicates the number of proteins, red bar as up-regulated and blue bar as down-regulated number of proteins.

List of Tables

Introduction

The role of inflammation in the development of cancer was described as early as 1863, it involves enhance of tumor growth and metastasis in different types of cancer; pancreatic, lung, gastric, breast and many others [1-4]. It has been revealed to affect phases of malignancy by modulating machinery contents in cellular proliferation, angiogenesis and tumor metastasis [5,6] accompanied by genetical and translational regulation of tumor suppressors or oncogene to favor the inflammatory conditions for the survival advantage. The increased risk in cancer by inflammation involves bioactive molecules, such as cytokines, growth factors, and chemokines, secreted from cells infiltrating tumor microenvironment [7]. For several pro-inflammatory cytokines like tumor necrosis factor-α (TNF-α), IL-8, IL10, and growth factors TGF-β, have been observed to increase in the tumor microenvironment [8-10].

Among, TNF-α is known to play dual role in oncoimmunology either acting as an anti-cancer factor or behaving as an immunosuppressive cytokine depending upon the stage and type of cancer [11,12]. This contributes to the maintenance of proinflammatory microenvironment by activation of NF-kB and IFN pathways and a high level of reactive oxygen species (ROS). TNF-α binds to its receptor TNF-R1 and recruits several adaptor proteins like TRADD, TRAF2, TAK1, and forms complex I and activates cell survival pathway through activation of NF-kB. On the other hand, where in case TNF-α inhibits NF-kB, complex II is formed and it activates caspase-8, leading

the cells to death. Previous research had observed that TNF−α induced NF−kB activation is responsible for cancer progression and metastasis in many types of tumors [13]. The increased level of TNF−α had been observed with poor prognosis, lymph node metastasis [14]. Altogether, suggesting the important role of TNF−α in breast cancer progression and metastasis. The study on TNF−α, however, is not well developed and we found needs to systematically investigate the modulation of change induced by TNF−α.

There is no doubt that the cellular energy system, which is complex and finely regulated, is responsible not only for forming the fuel necessary for cells' survival but also for other cellular processes specific according to the cell type [17]. Mitochondria are the essential powerhouse of the cell as ATP generating organelle undergoing complex metabolic network that involves a high degree of regulation [15]. Based on the recent studies, ut has been revealed that TNF−α regulates mitochondrial functions by modulating several regulators of the innate immune pathway [13,14], here, we have further investigated the association between the metabolic state and the response to cytokines in two different cell lines. Breast cancer had been broadly characterized as hormone responsive, estrogen receptor/progesterone receptor positive, representing early tumor benign condition whereas estrogen receptor/progesterone receptor/HER2 negative as aggressive and metastasis at a late stage. Metabolic reprogramming is an essential factor during cancer progression in solid tumors and metastasis to the preferred site. It is important to understand the differential

mechanisms involved in metabolic reprogramming in different types of breast cancer cells to understand its pathogenesis and selectively modulate cancer cell-specific pathways.

We have observed differential regulation of mitochondrial functions and its possible role in tumor progression that is mediated by TNF-α in different types of breast cancer cells; ER/PR positive and ER/PR/HER2 negative breast cancer cells. Using the high-resolution proteomics and targeted metabolomics, TNF-α modulated mitochondrial proteome and metabolites changes were observed. The research revealed that TNF-α differentially regulated the activity of mitochondria oxidative phosphorylation by the state change in ETC complex activity and assembly of the cells.

There are studies reporting a great amount of ubiquitin modification at the inner mitochondrial membrane (IMM) [18]. Ubiquitin is an 8.5 kDa peptide that covalently binds to lysine residues in a target protein, inducing localization, degradation, activity regulation, or promotion/inhibition of proteins interactions. This binding involves different enzymes to perform, referred to as E1, E2, and E3 ubiquitin ligases. E3 ubiquitin ligases usually create an isopeptide bond between a lysine of the target protein and the C-terminal glycine of ubiquitin. The mutations in a potential mitochondrial E3 ubiquitin ligase, F-box and leucine-rich repeat protein 4 (FBXL4), were found to induce mitochondrial encephalopathy associated with severe mitochondrial bioenergetics dysfunction [18]. In this study, we attempted to observe the ubiquitination action on mitochondrial

respiratory complexes located in IMM with proteomics profiling.

Altogether, in this article we demonstrated that the mitochondrial metabolism differs between two cell lines and goes through an alternative metabolism pathway under TNF-α treated condition. More specifically, we observed activity change of oxidative phosphorylation in the mitochondria with assembly change of electron transfer chain complexes under the treatment of TNF-α. We have revealed ubiquitin post-translational modification (PTM) as a potential modulating factor for the functional differences.

Materials and methods

1. Cell Culture, Pharmacological Treatments, and Transfection

MCF7 and MDA-MB231 cells were cultured in Dulbecco's Modified Eagle's Medium (DMEM, HyClone, Logan, UT, USA) containing 10% heat inactivated fetal bovine serum (FBS, HyClone) and 1% penicillin. Cells were grown at 37 ° C in an atmosphere of 5% CO2. The cells were treated with Human TNF-α (premium grade, Enzo, Farmingdale, NY, USA) in final concentration of 10ng/mL condition for 24 hours. MG132 (Sigma, St. Louis, MO, USA) was used at in final concentration of 10 μg/L, and 2-deoxy-glucose (2DG) was purchased from Sigma. Cells were transfected using HA-Ubiquitin vector from Addgene according to the manufacture's protocol.

2. Mitochondria isolation and western blot

Cells were seeded at 3×10^6 density and after overnight incubation cells were treated as indicated. Cells were washed three times with cold PBS and harvested. The cells were passed through 24 G syringe 30 times using mitochondria isolation buffer (0.25 M Sucrose, 10 mM Tris HCl and 1X protease inhibitor). After centrifugation at 600 g for 10 min, the supernatant was collected, and after the centrifuged at 8,000 g again, mitochondrial pellets were collected. The pallets were lysed with RIPA lysis buffer (Thermo Scientific, San Jose, CA, USA) with protease inhibitor (cOmplete; Roche Diagnostics, Mannheim, Germany), followed by a brief sonication on ice.

3. Immunoprecipitation of HA-tagged proteins

For the immunoprecipitation, EZ-viewTM Red Anti-HA affinity gel (Sigma) was used. The beads were equilibrated in lysis buffer by adding 750 ml of lysis buffer (RIPA and 1X protease inhibitor) to the tube, followed by vortex, centrifugation at 8,200 g for 30 seconds, and the supernatant was removed. The cell lysates were transferred into the tube of equilibrated EZ-viewTM Red Anti-HA affinity gel, and were incubated for 1 hour at 4 ° C using a shaker. The affinity gel was washed four times at in lysis buffer for 5 minutes each and then pelleted by centrifugation for 30 seconds at 8,200 g. The HA-fusion proteins were eluted by 100 μg/ml HA peptides (Sigma). The samples were incubated for 15 minutes at room temperature, and after a centrifugation the supernatant was collected.

4. Sample preparation and digestion

Protein concentration was determined by BCA assay kit (Thermo Scientific). Protein samples were fractionated on 4-12% Bis-Tris Gels (Invitrogen, Carlsbad, CA, USA) and stained with Coomassie Brilliant Blue (Sigma). Each gel lane was cut into ten pieces and subjected to in-gel tryptic digestion following the general protocol [19]. Briefly, protein bands were excised, distained, and washed further reduced with 20 mM DTT and alkylated with 55 mM iodoacetamide. After dehydration, the proteins were digested with 13 ng/μl sequencing-grade modified porcine trypsin (Promega, Madison, WI, USA) in 50 mM ammonium bicarbonate overnight at 37 ° C. Peptides were extracted from the gel slices in 50% ACN and 5% formic acid, and dried under vacuum.

5. LC-MS/MS analysis

Peptides were resuspended in 25 mL Solvent A (0.1% formic acid in water, pH 2) and 5 mL sample was loaded onto an analytic column (PepMap, 75 μm ID*50 cm 3 μm, ES803, Thermo Fisher Scientific) and separated with a linear gradient of 5-32% Solvent B (0.1% formic acid in ACN) for 150 minutes at a flow rate 300 nL/min. MS spectra were recorded on Q-Exactive (Thermo Fisher Scientific) interfaced with a UltiMate 3000 RSLCnano (Thermo Fisher Scientific). The standard mass spectrometric condition of the spray voltage was set to 1.5 kV and the temperature of the heated capillary was set to 250 ° C. The full scans were acquired in the mass analyzer at 400-1,400 m/z with a resolution of 70,000 and the MS/MS scans were obtained with a resolution of 17,500 by normalized collision energy of 27 eV for high-energy collisional dissociation fragmentation. The automatic gain control target was 5×10^4, maximum injection time was 120 ms, and the isolation window was set to 2 m/z. The Q-Exactive was operated in data-dependent acquisition (DDA) mode with one survey MS scan followed by ten MS/MS scans, and the duration time of dynamic exclusion was 20 s.

6. Database search

Collected MS/MS data were searched against the decoy UniProt human database (version 3.83, 186,578 entries) by Proteome Discoverer 2.2 (PD 2.2, Thermo Scientific) software. Precursor and fragment ion tolerance were set to 10 ppm and 0.5 Da, respectively. Trypsin was chosen as the enzyme with a maximum allowance of up to two missed cleavages.

Carbamidomethyl (+57.02 Da) of cysteine was considered as the fixed modification, while the variable modification was set for methionine oxidation (+15.99 Da) and GlyGly (+114.04 Da). The result filtration parameters of PD 2.2 were set as peptide and protein identifications at greater than 95% and 99% probability, respectively, as specified by the Peptide and Protein Prophet algorithm and if the protein identification contained at least two identified peptides with an false discovery rate ≤0.1%.

7. Relative protein quantification and bioinformatics analysis

Relative protein quantification was accomplished as spectral count label-free method. The spectral count data were normalized to compare the abundances of proteins between samples using PD 2.2 software. The normalized spectral counts from triplicate analyses of the MCF7 and MDA-MB231 cells treated or untreated with TNF-α were compared by power law global error model-signal to noise (PLGEM-STN) [20], Bioconductor package from R program (www.R-project.org) [21]. We filtered statistically significant proteins using 0.01 as a p-value threshold. Then we refined spectral counts of differentially expressed proteins (DEPs) within the range of 0.01 ≤ p-value ≤0.05, which were excluded from first criteria p-value <0.01, using moment adjusted imputation (MAI) equation [22] and finalized the list of DEPs with statistically significant change in their abundance. The subcellular localization and functional annotation of the DEPs were classified using Ingenuity Pathway Analysis (IPA, QIAGEN Inc., www.qiagenbioinformatics.com) and Protein Analysis through

Evolutionary Relationships Classification System (PANTHER, version 7.2, www.pantherdb.org) [23].

8. BN-PAGE separation

50 μg of mitochondrial pellets were solubilized as per manufacturer' s protocol [24] and BN-PAGE was performed on Native PAGE Novex 3%-12% Bis-Tris Protein Gels (ThermoFisher Scientific). In-gel enzyme activities of different oxidative phosphorylation complexes were analyzed on gradient Bis-Tris gel. For complex I, 1 mg NADH and 25 mg NTB was used in 2 mM Tris-HCl (pH 7.4) and for complex IV, 5 mg DAB and 10 mg cytochrome C in 50 mM potassium phosphate buffer (pH 7.4) was used for in gel activity.

9. Spectrophotometric analysis of mitochondrial Complex I and Complex II assays

The activity of mitochondrial complex I was analyzed spectrophotometrically. MCF7 and MDA-MB231 cells were seeded at the density of 5×10^5 cells in the 6-well plate. After overnight incubation, the cells were treated as indicated. The cells were harvested and washed with cold DPBS. The cells were subjected to 2-3 freeze-thaw cycles in a freeze-thaw complete solution (0.25 M sucrose, 20 mM Tris-HCl (pH 7.4), 40 mM KCl, 2 mM EDTA supplemented with 1 mg/ml fatty acid-free BSA, 0.01% Digitonin and 10% Percoll). The cells were washed again with the freeze-thaw solution devoid of digitonin and resuspended in Complex I assay buffer (35 mM potassium phosphate (pH 7.4), 1 mM EDTA. 2.5 mM NaN3, 1 mg/ml BSA, 2 μg/ml antimycin A, 5 mM NADH). The reaction

was started by adding 80 μg of cell lysate to 500 μl of assay buffer in 1 ml quartz cuvette. Complex I activity was measured for 3 minutes by monitoring the decrease in absorbance at 340 nm after the addition of 2.5 mM acceptor decylubiquinone indicating the oxidation of NADH.

Similarly, for Complex II activity, cells were seeded at density of 1.5×10^6/60mm dish. The cells were harvested and washed with cold DPBS. All the subsequent steps were performed at 4 ° C. The cells were suspended in 0.5 ml of 20 mM hypotonic potassium phosphate buffer (pH 7.5) and lysed using a 24 G syringe syringe and subjected to freeze-thaw cycle. The cell lysate (80 μg) was added to the 1ml of Complex II assay buffer (0.1 M potassium phosphate (pH 7.5), 50 mg/ml BSA, 100 mM NaN3, 200 mM succinate) and incubated in water bath for 15-20 minutes at 37 ° C. Complex II activity was measured for 6 minutes by monitoring the decrease in absorbance at 600 nm after the addition of 2.5 mM acceptor decylubiquinone and DCPIP.

10. ATP Assay

MCF7 and MDA-MB231 cells were seeded in density of 5×10^4 in 24-well plates. After overnight incubation desired treatments were given and ATP levels were measured in control and treatment conditions by an ATP dependent luciferase assay using ATP determination kit (Molecular Probes/Life Technologies, ON, Canada).

11. Metabolite extraction

9.0×10^6 of MCF7 and MDA-MB231 cells treated and untreated with TNF-α were washed once in ice-cold PBS and resuspended in 1mL of 80% methanol containing 20 mg/mL of isotopically labeled fructose 6-phosphate as an internal standard (Cambridge Isotope, Inc., Woburn, MA, USA). Cells were incubated at -80 ° C for 20 minutes and scrapped on dry ice. The cell lysate/methanol mixtures were centrifuged at 14,000 g for 3 minutes at 4 ° C and the metabolite containing supernatant were transferred to a new 1.5 ml tube. Following addition of 500 μl of 90% methanol to the remained pellets, the pellets were vortexed and centrifuged at 14,000 g for 3 minutes at 4 ° C. The metabolite containing supernatants were combined, filtered in 0.22 μm pore size, and dried. The dry metabolite extracts were reconstituted into 100 μL of 0.1% formic acid for targeted MRM-MS analysis.

12. Analysis of metabolites by LC-MRM

Extracted metabolites were analyzed by LC-MRM on Agilent 1290 Infinity HPLC series coupled with Agilent 6490 triple-quadrupole (QQQ) mass spectrometry (Agilent, Santa Clara, CA, USA). Chromatography separation was achieved on ZORBAX Eclipse Plus C18 column (2.1 x 150 mm, 3.5 μm particle size, Agilent) at a flow rate of 0.25 mL/min over 45 min gradient from 2% to 30% acetonitrile in 0.1% formic acid. In QQQ, the parameters were set to alternating negative and positive ionization mode, capillary voltage with 3500 V, fragment or of 130 V, ion source gas temperature of 250 ° C, nebulizer pressure of 50 psi, and sheath gas temperature of 350 ° C. Dynamic MRM scan type was used with 2 minutes of delta

retention time. Collision energies for each peptide were optimized by Skyline software (version 4.1.0, MacCoss Lab Software, University of Washington; skyline.gs.washington.edu) [25]. The MRM transitions for the analyses, collision energy (CE), and retention time are listed in Supplementary Table S2. The multiplexed MRM-MS analysis of metabolite transitions was performed in triplicate. The integration of peak areas for MRM transitions was calculated using Skyline software. The coefficient of variation (CV) of the integrated peak area for standard metabolite was determined by the ratio of the standard deviation to the mean of triplicate measurements. Each integrated peak area of MRM transition was calibrated to the standard metabolite, isotopically labeled fructose 6-phosphate.

13. Statistical analysis

BRCA patients in the 'The Cancer Genome Atlas (TCGA) database (https://peerj.com/articles/cs-67) were ranked by the level of NDUFB1, SDHA, COX7B and COX4I1 expression and divided into two groups; top quarter and low quarter in expression level. These groups were analyzed in Kaplan-Meier survival plot to estimate the correlation between gene's expression level and survival of patients using OncoLnc (http://www.oncolnc.org) [26]. Data are expressed as mean of + SEM of two or three independent experiments. Unpaired two-tailed Students t-test was performed. Graphpad prism was used to perform all statistical analysis. The TIMER database is a web resource used for systemic analysis and evaluation of clinical impacts of different immune factors and immune cells in diverse cancer types [27].

Results

1. Proteomics Analysis of MCF7 and MDA-MB231 under TNF-α treated and untreated conditions

Aiming to identify DEPs between ER/PR positive and ER/PR/HER2 negative breast cancer cell lines associated with response to cytokine TNF-α, we have treated TNF-α to MCF7 and MDA-MB231 breast cancer cell lines, and isolated mitochondria organelle from the cells. The mitochondria samples were separated and digested in-gel and we performed triplicate LC-MS/MS analysis on the Q-Exactive as the workflow described (Figure 1A). Overall, 1,244 protein groups were quantified as mitochondria proteins (95% confidence on peptide level and 99% confidence on protein level), 1,077 and 1,150 mitochondria proteins were identified at MCF7 and MDA-MB231 respectively; there were no major differences in coverage between TNF-α treated or untreated conditions (Figure 1B). The identified proteins were analyzed with statistical analysis method as described in methods for the selection of statistically confident and significant DEPs (Figure 1C). In specific, the PLGEM-STN analysis was conducted on 1,244 proteins for p-value calculation, the spectral count value of each protein group acquired from mass spectrometry was refined by MAI normalization method, then the p-value of the refined spectral count was calculated with PLGEM-STN method once again. Finally, proteins with p-value <0.01, 108 proteins in MCF7 and 111 proteins in MDA-MB231 respectively, were selected as DEPs (Table S1). For the MCF7 there were 62 up-regulated

and 49 down-regulated DEPs and for MDA-MB231 there were 81 up-regulated and 27 down-regulated DEPs. From the volcano plot, we have noticed proteins of electron transfer complex, such as NDUFA11, COX7C, NDUFS3, LYRM7, and COX16, showed a high degree of expression change (Figure 1D).

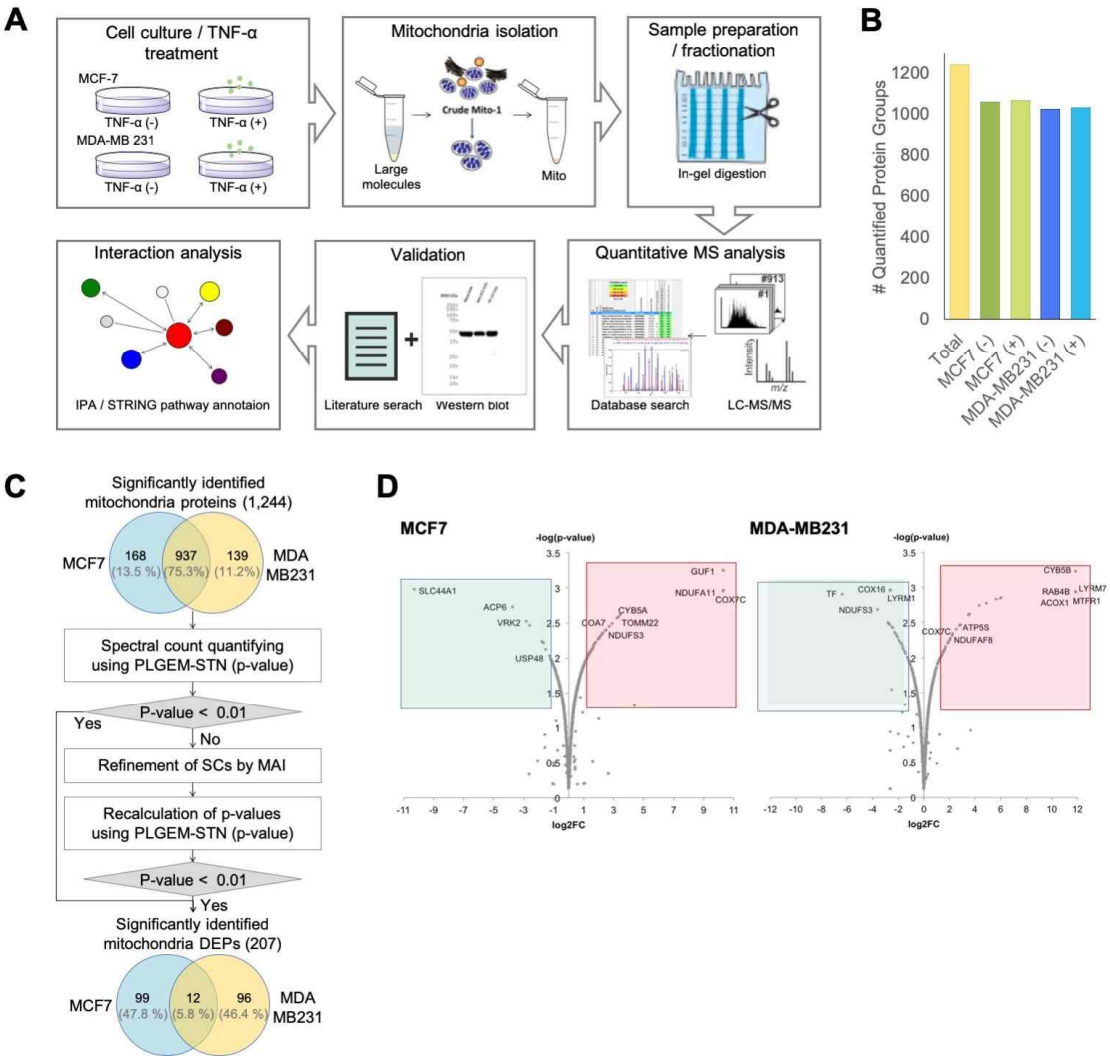

Figure 1. Proteomics of TNF-α regulated mitochondrial proteins in MCF7 and MDA-MB231 breast cancer cells. *(A) Workflow of mitochondria global profiling. The mitochondria were isolated and proteins were trypsin-digested in gel. We used liquid chromatography coupled with the Q Exactive followed by computational analysis in Proteome Discoverer 2.2 and IPA. (B) Total number of proteins quantified in each group of samples. (C) Workflow of statistical criteria for DEP selection. (D) Volcano plots of proteins displayed in the p-value (-log10)*

versus signal-to-noise ratio (STN). The p-value and STN were determined by PLGEM-STN statistical analysis for label-free quantification, proteins in red box were up-regulated and in blue were down-regulated.

2. Functional Analysis of MCF7 and MDA-MB231 under TNF-α treated and untreated conditions

The initial bioinformatic analysis examined the functional differences between two cell lines had between TNF-α treated and untreated conditions. We first composed the pie-chart of proteins according to their Kyoto Encyclopedia Genes and Genomes (KEGG) pathway annotations and found a striking dominance of metabolic process on four charts of the two treatments in two cell lines (Figure 2A). To identify inversely differentiated pathways between MCF7 and MDA-MB231, the DEPs were clustered using hierarchical clustering analysis (Mev software) and the major functions of a cluster were analyzed by IPA (Figure 2B). Cluster 1, which is a group of DEPs up-regulated in MCF7 and down-regulated in MDA-MB231, was majorly involved in PPARα/RXRα activation, pyrimidine deoxyribonucleotides De Novo biosynthesis, and salvage pathways of pyrimidine ribonucleotides. On the other hand, Cluster 2, which is a group of DEPs down-regulated in MCF7 and up-regulated in MDA-MB231, was involved in mitochondrial dysfunction, sirtuin signaling pathway, oxidative phosphorylation, oxidative ethanol degradation, fatty acid α-oxidation, TCA cycle, and glutamate biosynthesis. Altogether, these two results suggest that the TNF-α treatment incurred differential metabolic shifts in both cell lines.

From the analysis, we have attained the list of proteins associated with metabolism and conducted network analysis using STRING database and Cytoscape visualization software (Figure 1C). We have visualized the network of the metabolism-related proteins and the network analysis showed that they are associated with mitochondrial translation, generation of precursor metabolites and energy, nucleotide metabolic process, ATP metabolic process, protein-containing complex subunit organization, respiratory electron transport chain, mitochondrial respiratory chin complex assembly, and fatty acid oxidation. The enriched pathways were majorly involved in two functions, which are energy production pathways and regulation of building blocks (enriched with FDR <0.01). Interestingly, the MCF7 proteins involving in mitochondrial translation and protein-containing complex subunit organization, showed down-regulating trends, whereas two pathways showed up-regulating trends in MDA-MB231. We have inferred from the change patterns that the functional annotation indicates the alternation in electron chain complexes,

We have also annotated the functions of selected DEPs MCF7 and MDA-MB231. The annotation showed MCF7 and MDA-MB231 majorly involved in mitochondrial dysfunction, oxidative phosphorylation, and sirtuin signaling pathway. Interestingly proteins related to mitochondrial dysfunction and oxidative phosphorylation were all up-regulated, whereas MCF7 showed neutral regulation on both up and down (Figure 1D). Altogether, these analyses highlight that differences in mitochondrial metabolism after the cytokine treatment are

generally associated with the change in ATP production by oxidative phosphorylation, which is operated by ETC complex. We have further validated such observed alteration with more bioinformatic analysis and molecular assays.

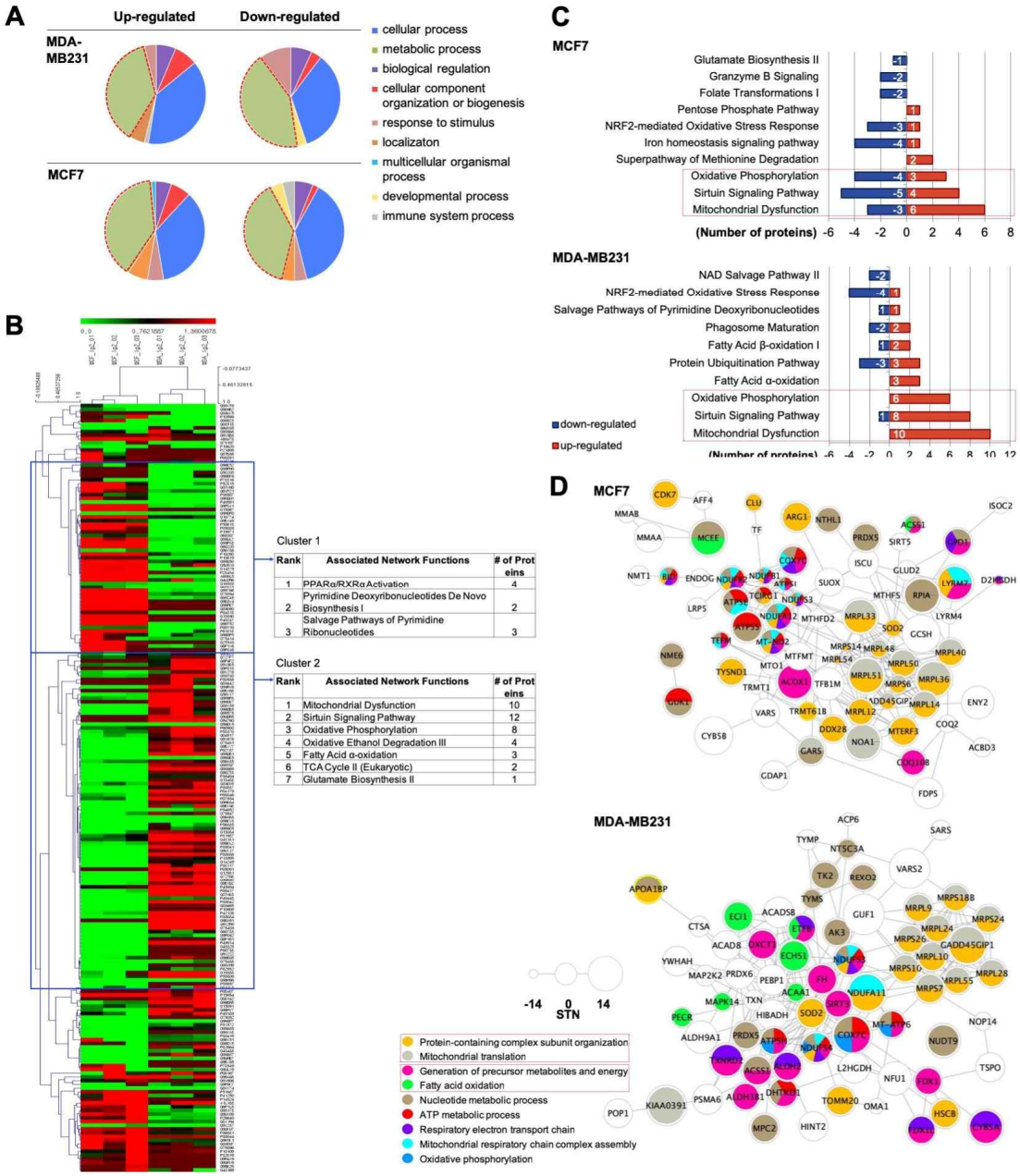

Figure 2. Functional differences between MCF7 and MDA-MB231 treated with TNF-α. *(A) Functional enrichment of cellular processes by DEPs categorized using IPA tool. (B) Hierarchical clusters of DEPs by MEV. The red indicates up-regulation and blue indicates down-regulation after TNF-α*

treatment. (C) Functional annotation enrichment by DEPs. The x-axis indicates the number of proteins, red bar as up-regulated and blue bar as down-regulated number of proteins. (D) Interaction network of DEPs enriching metabolism process. The size of node indicates up/down-regulated ratio of proteins after the TNF-α treatment.

3. The targeted metabolomics analysis on metabolic pathways in MDA-MB231 and MCF7 under the TNF-α treated and untreated conditions

We have measured the differentiated levels of 18 target metabolites (glucose-6-phosphate (G6P), ribose-5-phosphate (R5P), fructose-6-phosphate (F6P), fructose-1,6-phosphate (F1,6BP), glyceraldehyde-3-phosphate (GA3P), dihydroxyacetone phosphate, pyruvate, lactate, citrate, aconitate, iso-citrate, α-ketoglutarate, glutamate, succinate, fumarate, malate, oxaloacetate, and aspartate) involving in glycolysis/glycogenesis and TCA cycle to understand the metabolic adaptation after the TNF-α treatment. The metabolites from MCF7 and MDA-MB231 cells were extracted and their change in level was measured by Agilent QQQ mass spectrometry. As we anticipated, the metabolites of glycolysis/glycogenesis and TCA cycle flux differed between two cell lines (Figure 3A and Table S4).

For the MCF7, the level of metabolites involving in glycolysis/glycogenesis and TCA cycle decreased in TNF-α treated condition, and the accumulation of glutamate was observed. For MDA-MB231 cell, the accumulation of

fructose−1,6−phosphate and 3−phosphoglycerate were observed, the level of ribose−5−phosphate, which is an precursor metabolite for the pentose phosphate pathway for the nucleotide biosynthesis, showed significant up−regulation, and pyruvate and aspartate, which is electron acceptors, showed significant up−regulation. The level of α−ketoglutarate, which is a precursor of the oncometabolite 2−HG, was significantly up−regulated, the succinate, which is also oncometabolite, was accumulated.

Along with glycolysis/glycogenesis and TCA cycle, we observed the accumulation of different metabolites important for the nucleotide balance. It has been reported that ER negative cells rely on glutamine uptake for amino acid metabolism, whereas ER positive cells produce more glutamine through the activity of glutamine synthetase [36,37]. The result showed down−regulated glutamate and accumulation of aspartate and α−ketoglutarate in MDA−MB231, indicating the increased uptake of glutamine, whereas MCF7 produces Glutamine. Altogether, we could come up with a summary that MCF7 may use TCA cycle after the TNF−α treatment and generate glutamate. On the other hand, the MDA−MB231 cells may not focus on producing ATP, leading to accumulation of TCA metabolites.

To elaborate the metabolomics data we attained, we have integrated the functional analysis done by proteome and metabolome annotation (Figure 3B). Interestingly, the protein expression trends on glycolysis increased in MCF7 whereas it was decreased in MDA−MB231, and the metabolite abundance

trend was exact opposite, decrease in MCF7 and increase in MDA-MB231 as the metabolites accumulated. The pathway in building block synthesis, aspartate biosynthesis, and glutamate degradation showed exact opposite trends in both proteins and metabolites. The integrated analysis also indicated opposite regulation on oxidative phosphorylation-related processes.

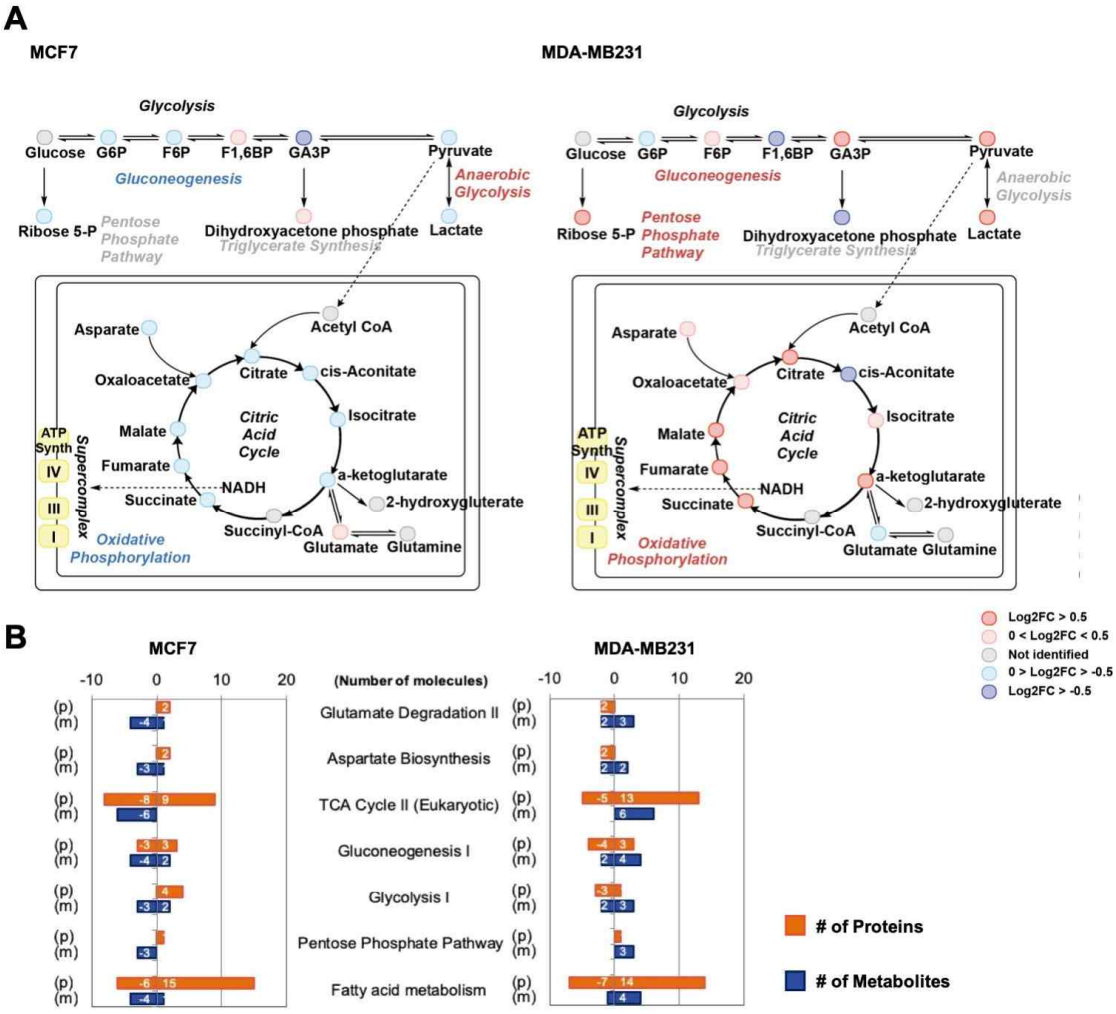

Figure 3. The level of differentially regulated metabolites under the TNF-α treated condition in MCF7 and MDA-MB231 cells. *(A) Targeted metabolomics analysis of 18 metabolites (glucose-6-phosphate (G6P), ribose-5-phosphate (R5P), fructose-6-phosphate (F6P), fructose-1,6-phosphate (F1,6BP), glyceraldehyde-3-phosphate (GA3P), dihydroxyacetone phosphate, pyruvate, lactate, citrate, aconitate, iso-citrate, α-ketoglutarate, glutamate, succinate, fumarate, malate, oxaloacetate, and aspartate) related to glycolysis and TCA cycle in MCF7 and MDA-MB231 in the presence and absence of*

TNF-α. (B) Functional enrichment of metabolism processes and the up/down-regulation of proteins and metabolites.

4. Identification of change in oxidative phosphorylation differentially regulated by TNF-α

We have observed the alteration of oxidative phosphorylation related proteins and metabolites of MCF7 and MDA-MB231 in presence of TNF-α. To visualize the distribution of all the oxidative phosphorylation related functions (p-value <0.001, Fisher's exact test) in two cell lines, a bubble chart was used (Figure 4A). The chart showed apparent difference on metabolism of reactive oxygen species, production of reactive oxygen species, degradation of hydrogen peroxide, energy production, and lipid metabolism. The result was in agreement with the previous functional analysis, giving us the further evidence that there are opposite differential alterations in oxidative phosphorylation on two cell lines.

The oxidative phosphorylation results in uneven distribution of protons between mitochondria intermembrane space and matrix of mitochondria, and such proton distribution generates a pH gradient and a transmembrane electrical potential that creates a proton-motive force. When protons flow back to the mitochondrial matrix through an enzyme complex 5, the ATP is synthesized. Such electron gradient is formed by ETC complex, which is a series of complexes composed of complex 1, 2, 3, 4, and 5 that transfer electrons from electron donors to electron acceptors via redox [57]. Thus, the ETC complex is a major modulator of the mitochondrial ATP production induced by

oxidative phosphorylation. Here, we aimed to reveal what causes the differential regulation on oxidative phosphorylation and how ATP production level differs between two cell lines after the TNF-α treatment.

Firstly, in order to observe how the oxidative phosphorylation alters, we have observed the ETC complex activation. We have used BN-PAGE to measure the assembly change of ETC complex, especially to observe cluster alteration of super-complex (SC). Among ETC's 5 complexes, the SC is an assembly found in the form of Complex I/III, Complex I/III/IV, and Complex III/IV. The stable SC formation is known to reduce oxidative damage and increase metabolism efficiency, which means the assembly forms the electron gradient leading to generation of ATP [58].

The BN-PAGE result showed the assembly decrease of SC after TNF-α treatment, and it was observed with a higher degree of decrease in MDA-MB231 than MCF7 cells (Figure 4B). This observation was further supported by protein abundance measurement conducted by LC-MS/MS. We have isolated complex III and IV that do not form rigid SC assembly and measured their abundance differences after the TNF-α treatment. The result showed a mild change in abundance of complex III and IV proteins of MCF7, whereas the abundance of complex III and IV increased significantly in MDA-MB231 (Figure 4C). As a conclusion, the assay and proteomics showed that the assembly of SC in MDA-MB231 are disturbed, whereas MCF7 showed no significant change, providing a possible

rationale behind the OMICS analysis results that showed decreased ATP producing related pathways in MDA-MB231, whereas increase in MCF7 after the TNF-α treatment.

Next, we have measured the activity of the individual complex. We have measured the change of level of NADH oxidized to measure the functional up and down of complex I of cells in TNF-α or 2DG, which inhibits the glycolysis of the cell, treated condition. The result suggested that for the MDA-MB231, TNF-α decreased the activity of complex I as we anticipated, and we have found out that the glycolysis step is essential for maintaining the function of complex I. On the other hand, inhibition of glycolysis increased the activity of complex I in MCF7 cells. The NADH dehydrogenase activity decreased in TNF-α treated cells, also decreased in 2DG treated condition. The MCF7 cell, however, remained with no significant change under the TNF-α treated condition and increased activity under the 2DG treated condition (Figure 4D).

We have measured the level of succinate oxidized to observe activity change of complex II of cells in TNF-α or 2DG treated condition. For the MDA-MB231 cells, the level of succinate oxidized slightly decreased under the presence of TNF-α, however, it significantly increased under the presence of 2DG. The MCF7 cells showed a slight increase in oxidized succinate in the presence of TNF-α and 2DG (Figure 4E). We also have measured the activity of complex III. For MDA-MB231, the activity decreased under the TNF-α as we anticipated, whereas remained the same in MCF7. The proteomics and assay results

suggest that TNF-α alters the level of complex I in MCF7 however still can maintain the level of complex I activity. On the contrary, the complex I and III in MDA-MB231 decreased in activity with the alteration in some of the critical components under the TNF-α treated condition.

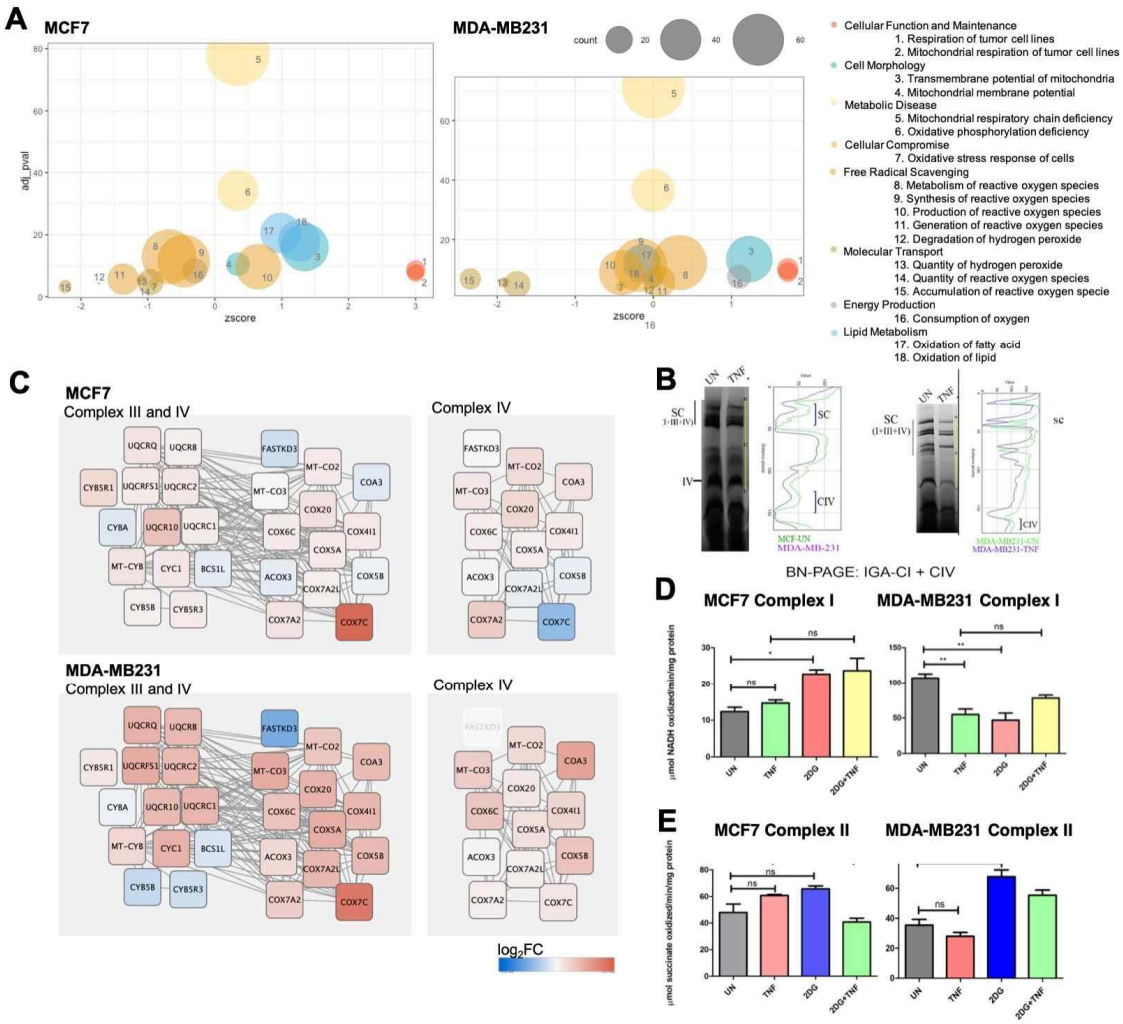

Figure 4. The assembly and activation of oxidative phosphorylation under the TNF-α treated condition in MCF7 and MDA-MB231 cells. *(A) Functional analysis showing ATP related functions in MCF7 and MDA-MB231. (B) MCF7 and MDA-MB231 cells were treated with TNF-α (10 ng/μl) for 24 h with or without MG132 (10 μM) for 8 h. After treatment, mitochondria fraction was isolated and further analyzed by BN-PAGE and in-gel enzyme staining as described in Methodology. (C) The biological network analysis of complex proteins of MDA-MB231 under TNF-α treatment. Associations*

among proteins are shown by gray lines, which represent direct or indirect interactions. Up-regulated proteins are shown in red, and down-regulated proteins are shown in blue. (D) and (E) MCF7 and MDA-MB231 cells were treated with TNF-α (10 ng/μl) and 2DG (10 mM) either alone or in combination for 24 h and complex I and complex II activity was measured spectrophotometrically.

5. Identification of change in ATP production differentially regulated by TNF-α

We have observed the mitochondiral oxidative phosphorylation function decreased in MDA-MB231, whereas there was no significant change in MCF7 under TNF-α treated condition. To verify the observation, we have measured the level of mitochondria generated ATP and total ATP (Figure 5A). We also treated 2DG, which inhibits glycolysis, as control to confirm whether the ATP generation change is induced by the deficiency in oxidative phosphorylation complex.

For MDA-MB231, there was a significant decrease in mitochondria generated ATP levels of MDA-MB231 after the TNF-α treatment, and when treated with TNF-α and 2DG, the ATP generation level decreased, meaning that the TCA cycle does not act as an alternative path to generate mitochondria generated ATP under the stress condition. The total ATP level also decreased, altogether meaning that MDA-MB231 depends on mitochondrial generated ATP and the total ATP level decreased as cells were treated with TNF-α. On the other hand, the level of mitochondrial generated ATP increased in

MCF7 after the TNF-α treatment, and when treated with TNF-α and 2DG, ATP generation level increased, meaning that the TCA cycle can act as an alternative path to generate ATP under the stress condition in contrast to MDA-MB231. The total ATP level had no significant change, altogether meaning that MCF7's level of ATP is not affected by the treatment of TNF-α.

Altogether, we have observed the differential regulation on oxidative phosphorylation-related processed both on proteomics and metabolomics data. With the given observation, we have validated oxidative phosphorylation was differentially regualted in two cell lines after the treatment of TNF-α by assay showing that the assembly of SC and the activity of ETC complex changed, and the alteration led to ATP generation change. With the treatment of TNF-α, the SC assembly and activity of ETC complex were not significantly altered in MCF7, and the level of mitochondria generated ATP increased. On the other hand, the SC assembly and activity of ETC complex decreased in MDA-MB231, and the level of mitochondria generated ATP decreased.

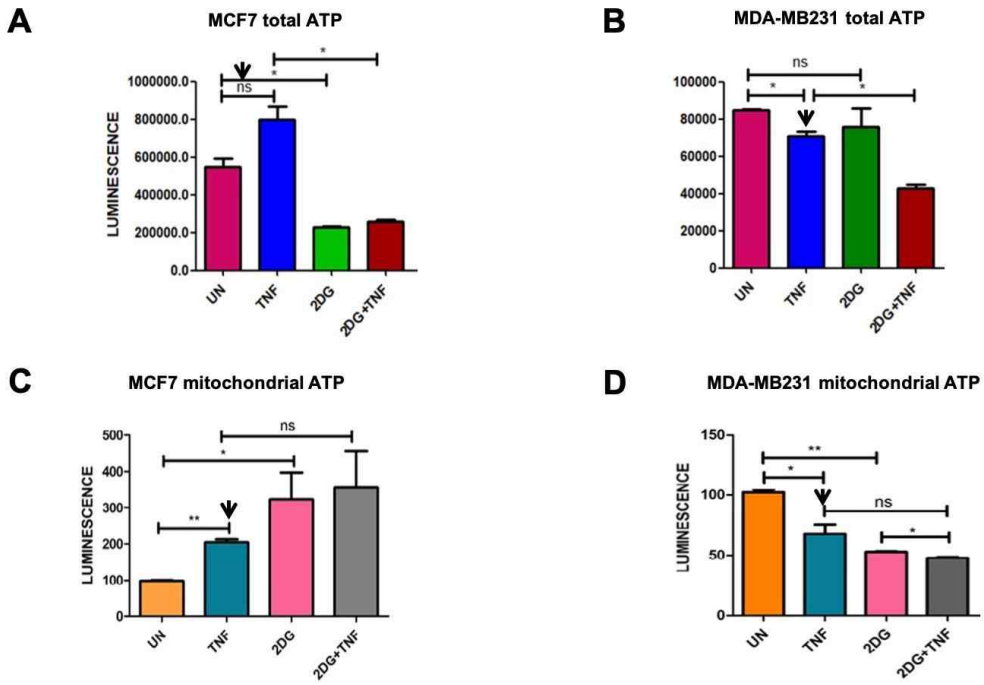

Figure 5. The level of differentially regulated ATP. (A) and (B) MCF7 and MDA-MB231 cells were treated with TNF-α alone or in combination with 2DG (10 mM) and the steady-state ATP levels were determined by luciferase-based assay as described in Methodology. (C) and (D) MCF7 and MDA-MB231 cells were treated with TNF-α alone or in combination with 2DG (10 mM) and the mitochondria generated ATP levels were determined.

6. The change of ubiquitin PTM in ETC complex is differentially regulated by TNF-α

With an aim to identify proteins or modification that leads to disassembly of SC, we have measured the protein abundances modulated by ubiquitin PTM. We have enriched the ubiquitin-modified peptides and quantified their change in abundance after the TNF-α treatment. For MCF7, 420 ubiquitinated proteins were identified, and for MDA-MB231, 127

ubiquitinated proteins were identified. The ubiquitinated proteins of MCF7 majorly involved in EIF2 signaling, sirtuin signaling pathway, and mitochondria dysfunction. MDA-MB231 majorly involved in EIF2 signaling, sirtuin signaling pathway, and mTOR signaling (Figure 7B). There were 16 reversely regulated proteins on ETC complex (Figure 7A).

NDUFS3, which is a part of N module, was one of the differently ubiquitinated proteins in two cell lines. NDUFS3 was significantly decreased in MCF7 cells and increased MDA-MB231 in the presence of TNF-α (Figure 2A). The ubiquitinated NDUFS3, however, was increased in MCF7 and decreased in MDA-MB231. The results suggest that TNF-α induced the ubiquitin modification to NDUFS3, thus, differentially regulated.

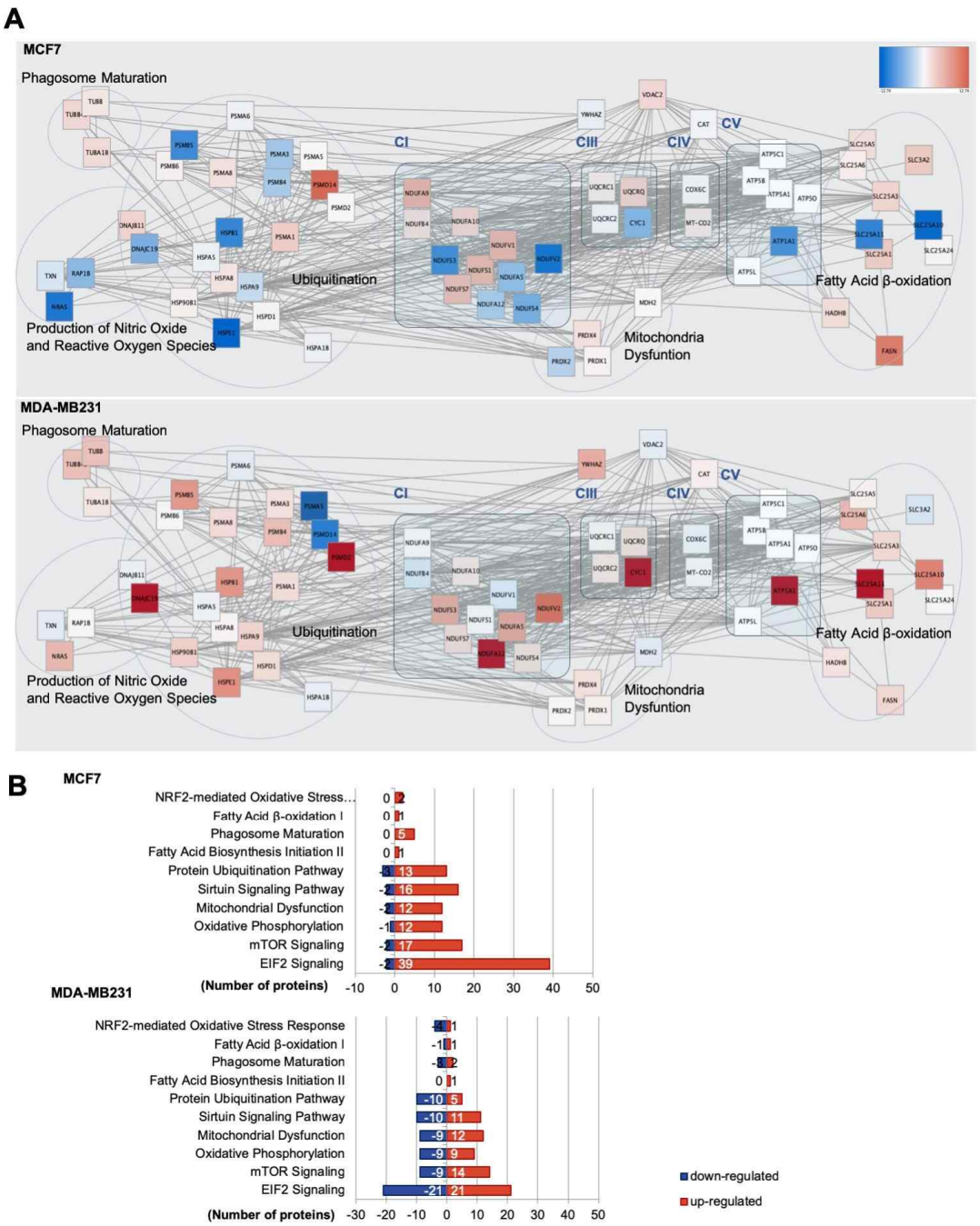

Figure 6. Differentially regulated ubiquitinated proteins. *(A) The biological network analysis of DEPs. Associations among DEPs are shown by gray lines, which represent direct or indirect interactions. Up-regulated proteins are shown in red, and*

down-regulated proteins are shown in green. (B) Molecular functions of DEPs by IPA tool. The x-axis indicates the number of proteins, red bar as up-regulated and blue bar as down-regulated number of proteins.

Discussion

The metabolism of tumor and the tumorigenesis generated by metabolic adaptation has been emerging hallmark of cancer. In the recent year, it has been evident that the metabolic adaptations differ dramatically between cancer types. The metabolism of ER positive primary breast tumors has been well characterized as reduced glycolysis, increased cellular respiration, increased breakdown and reduced synthesis of fatty acids, reduced glycolytic branching to pentose phosphate pathway and serine synthesis, and decreased uptake and increased production of glutamine [38]. On top of that, it has been revealed that cancer cells also modulate energy metabolism within the cancer microenvironment [39]. The microenvironment of tumors is formed by stromal cells, blood vessels, and the immune system via paracrine factors [40]. The inflammation involves enhancing tumor growth and metastasis in different types of cancer, and is known to affect phases of malignancy by modulating machinery contents in cellular proliferation, angiogenesis and tumor metastasis [5,6]. Likewise, there are emerging need to better identify the molecular basis of breast cancer initiation and progression and their metabolism adaptation according to types and progresses, in order to design targeted, molecular-based therapies.

The power-house of cell, mitochondria is ATP generating organelle undergoing complex metabolic network that involves a high degree of regulation [15] and it plays important role in many other cellular processes such as biogenesis. The cytokines

and growth factors responsible for forming tumor microenvironment is known to modulate the mitochondrial bioenergetics, thus, induce the formation of macromolecule that are required for the tumor growth. Among the cytokines, TNF-α is know to promote anti-tumor effects when it is specifically delivered to tumor sites [41,42], and the overexpression of TNF-α is known to result in long-term tumor growth suppression also [43]. TNF-α is actively being attempted to utilize on clinical application of cancer also, however, the differential role in regulation, especially of mitochondrial functions, in different type of breast tumor cells is not well understood. In order to identify the differential regulation of TNF-α, in this study, we have conducted proteomics and metabolomics characterization of mitochondrial proteome in two different cell types MCF7: hormone responsive early tumor conditions representing benign conditions and MDA-MB231 cells representing aggressive and metastatic conditions tumor cell types.

The analysis on mitochondria of two cell lines using high-resolution proteomics clearly indicated that TNF-α differentially modulates mitochondrial proteome. The proteins involving oxidative phosphorylation showed up-regulated property in MDA-MB231, and this could be an indication that oxidative phosphorylation could act as an alternative source of power to serve the high demand of cellular respiration. We have further focused on the activity and assembly of mitochondrial respiratory chain complexes differentially regulated in MCF7 and MDA-MB231 cells.

The complex I is consisted of two functional modules; an electron input module (N module) and an electron output module (Q module) [44]. The N module contains NADH oxidation, and the electrons generated are transferred via FMN and a series of Fe-S clusters to ubiquinone, creating electron concentration gradient [45]. For the complex I, the core units ND2 and ND3 [46], increased in MCF7 whereas remain significantly unaltered in MDA-MB-231 cells. The increase in abundance could have implied more activity as NADH Coenzyme Q oxidoreductase, which can explain the increase of mitochondrial ATP formation in MCF7 cell after the TNF-α treatment.

The complex II couples two major pathways in mitochondria, TCA cycle and respiratory chain, both being essential for oxidative phosphorylation. The complex II is also responsible for dehydrogenizing succinate, which is a potent oncometabolite [47] that signal the elevation in HIF-1α concentration, and signal leading to inhibition of histone demethylases (HDM) [48]. The activity complex II decreased in MDA-MB231 after the TNF-α whereas remain significantly unaltered in MCF7. The accumulation on succinate was observed in MDA-MB231, which in turn supported with earlier observation where decreased complex II had been observed in the tumor cells as compared to normal human mammary epithelial cell [49]. The accumulation of succinate on MDA-MB231 could also suggest that it may activate this epigenetic programming favoring the aggressive and metastasis of the breast cancer. The HIF-1α elevation due to the inhibition in prolyl hydroxylases made by succinate, leads to

increased angiogenesis and tumor vasculature [50]. The elevations in histone methylation due to the inhibition in HDM lead to epigenetic regulation of gene expression in a way that provokes carcinogenesis [51].

The complex III transfer the electron using Iron sulfur (Fe-S) clusters, which is an essential cofactors required for the electron transport in respiratory chain complexes. The deficiency in complex III is known to decreases NAD+ levels, resulting in diminished aspartate, which is necessary for cancer cell proliferation [52,53]. We have observed the LYRM7 proteins being oppositely regulated; decreased level of assembly factor LYRM7 in MDA-MB231 whereas increased at MCF7. We fond that there were recent study result suggesting that the binding of chaperone HSC20 to LYRM7 and UQCRFS1, existing on the mitochondrial matrix area, facilitates Fe-S cluster transfer to UQCRFS1, hence inducing the assembly of complex III and its function as electron transfer [54]. Such decrease in LYRM7 in MDA-MB231 could strongly suggest that deficient incorporation of Fe-S complexes in mitochondrial electron transport chain may have resulted in function of respiratory chain. The evidence of sub complexes observed in MDA-MB231 in presence of TNF-α also supports reduced the function of respiratory chain.

We observed alteration on metabolism, the major differences on metabolism found between ER positive and ER negative breast cancer cells were their dependency on glycolysis. The MCF7 adapted from glycolysis to TCA cycle under the stress condition, whereas for MDA-MB231 TCA cycle was not an alternative

pathway when the glycolysis was inhibited. Along with metabolic adaptation, we observed as accumulation of different metabolites important for the nucleotide balance. It has been reported that ER negative cells rely on glutamine uptake for amino acid metabolism, whereas ER positive cells produce more glutamine through the activity of glutamine synthetase [55,37]. The glutamate act as a precursor for the aspartate biosynthesis along with glucose, and aspartate acts as a fuel in TCA to generate intermediates like oxaloacetate or used in nucleotide biosynthesis in proliferating cells [56].

We, therefore, propose the notion that ER positive and negative tumors adapt to stress by different ways. The MDA-MB231 cells rely strongly on TCA cycle for ATP production. The TNF-α strongly disturb the SC of ETC complex, resulting in decreased ATP production, and increase up take of glutamine, resulting in higher colony forming ability. The MCF7 cells rely on glycolysis for energy production by freely reprograms to TCA cycle under TNF-α treated condition.

In conclusion, our study has helped understanding the differentially regulated behavior of the ER/PR positive and ER/PR negative in tumor microenvironment where the level of TNF-α is high. These data provide functional insights regarding tumorigenic potential of two different types of breast cancer cells, which differs in metabolism, function of mitochondria, and biogenesis of building blocks. The analysis on two breast cancer types provided a unique view of breast cancer, highlighting the complexity and phenotypic variability of this disease. This study

can be extended to understand metabolic reprogramming according to complex tumor microenvironment with different sole or mixture of cytokines. This study emphasize the fact that breast cancer subtypes differ in metabolic characteristics and study may identify novel factors that modulate metabolic reprogramming as therapeutic target to prevent the progression of aggressive breast cancer cells.

Table S1: The list of mitochondria DEPs in MCF7 and MDA-MB231 after the TNF-α treatment. *(A) List of 108 DEPs in MCF7, (B) and list of 111 DEPs in MDA-MB231.*

Gene name	Accession	Description	TNF_vs_CON_STN	TNF_vs_CON_p-val	log2FC
ASB9	Q96DX5	Ankyrin repeat and SOCS box protein 9	-13.6499	0.0012	-11.8727
COX16	Q9P0S2	Cytochrome c oxidase assembly protein COX16 homolog, mitochondrial	-13.6479	0.0012	-10.2877
D2HGDH	Q8N465	D-2-hydroxyglutarate dehydrogenase, mitochondrial	-13.6479	0.0012	-10.2877
MRPS14	O60783	28S ribosomal protein S14, mitochondrial	-13.6479	0.0012	-10.2877
MRPL54	Q6P161	39S ribosomal protein L54, mitochondrial	-13.6479	0.0012	-10.2877
MTHFS	P49914	5-formyltetrahydrofolate cyclo-ligase	-13.6479	0.0012	-10.2877
LYRM1	O43325	LYR motif-containing protein 1	-13.6479	0.0012	-10.2877
TF	P02787	Serotransferrin	-12.5911	0.0013	-6.3841
TRMT1	Q9NXH9	tRNA (guanine(26)-N(2))-dimethyltransferase	-9.9231	0.0022	-2.0430
LYRM4	Q9HD34	LYR motif-containing protein 4	-8.4592	0.0034	-2.8250
PET117	Q6UWS5	Protein PET117 homolog, mitochondrial	-8.3642	0.0035	-2.1965
ARL2	P36404	ADP-ribosylation factor-like protein 2	-8.1107	0.0036	-2.6633
NDUFS3	O75489	NADH dehydrogenase [ubiquinone] iron-sulfur protein 3, mitochondrial	-7.7401	0.0039	-2.5003
ATP5I	P56385	ATP synthase subunit e, mitochondrial	-7.5714	0.0041	-2.4284
ISOC2	Q96AB3	Isochorismatase domain-containing protein 2	-7.1786	0.0047	-2.2672
RAI14	Q9P0K7	Ankycorbin	-7.0452	0.0049	-1.2158
CPSF4	O95639	Cleavage and polyadenylation specificity factor subunit 4	-6.8300	0.0051	-0.5476
NIF3L1	Q9GZT8	NIF3-like protein 1	-6.6690	0.0054	-2.0686
HP	P00738	Haptoglobin	-6.3951	0.0060	-1.9660
SIRT5	Q9NXA8	NAD-dependent protein deacylase sirtuin-5, mitochondrial	-6.0820	0.0065	-0.2692
COQ2	Q96H96	4-hydroxybenzoate polyprenyltransferase, mitochondrial	-5.8987	0.0067	-1.7870
GADD45GIP1	Q8TAE8	Growth arrest and DNA damage-inducible proteins-interacting protein 1	-5.8740	0.0067	-1.7785
MMAB	Q96EY8	Cob(I)yrinic acid a,c-diamide adenosyltransferase, mitochondrial	-5.6191	0.0072	-1.6895
TEFM	Q96QE5	Transcription elongation factor, mitochondrial	-5.5343	0.0079	-1.6603
NDUFB1	O75438	NADH dehydrogenase [ubiquinone] 1 beta subcomplex subunit 1	-5.4946	0.0079	-1.6469
SOD2	P04179	Superoxide dismutase [Mn], mitochondrial	-5.4589	0.0080	-1.6344
CLU	P10909	Clusterin	-5.2010	0.0085	-1.5477
AKR7A2	O43488	Aflatoxin B1 aldehyde reductase member 2	-5.1380	0.0086	-0.9425
HSPA2	P54652	Heat shock-related 70 kDa protein 2	-4.9311	0.0091	-1.4582
MRPL48	Q96GC5	39S ribosomal protein L48, mitochondrial	-4.9110	0.0092	-1.4517
NOS1AP	O75052	Carboxyl-terminal PDZ ligand of neuronal nitric oxide synthase protein	-4.9025	0.0092	-1.4487

AFF4	Q9UHB7	AF4/FMR2 family member 4	−4.8464	0.0094	−0.8463
TRMT61B	Q9BVS5	tRNA (adenine(58)−N(1))−methyltransferase, mitochondrial	−4.8240	0.0094	−0.8390
ACBD3	Q9H3P7	Golgi resident protein GCP60	−4.4815	0.0106	−1.3129
MTHFD2	P13995	Bifunctional methylenetetrahydrofolate dehydrogenase/cyclohydrolase, mitochondrial	−4.3477	0.0109	−1.2705
BCAP31	P51572	B−cell receptor−associated protein 31	−4.2758	0.0111	−1.2477
TCIRG1	Q13488	V−type proton ATPase 116 kDa subunit a isoform 3	−4.1188	0.0117	−1.1984
ENDOG	Q14249	Endonuclease G, mitochondrial	−4.0156	0.0120	−1.1664
ACSS1	Q9NUB1	Acetyl−coenzyme A synthetase 2−like, mitochondrial	−3.9422	0.0123	−1.1435
KIF1BP	Q96EK5	KIF1−binding protein	−3.9372	0.0123	−1.1420
MRPS6	P82932	28S ribosomal protein S6, mitochondrial	−3.9169	0.0124	−1.1356
MGST1	P10620	Microsomal glutathione S−transferase 1	−3.8843	0.0125	−0.5414
GLUD2	P49448	Glutamate dehydrogenase 2, mitochondrial	−3.8468	0.0127	−1.1141
MTO1	Q9Y2Z2	Protein MTO1 homolog, mitochondrial	−3.8273	0.0128	−1.1082
NUDT8	Q8WV74	Nucleoside diphosphate−linked moiety X motif 8	−3.6056	0.0137	−1.0402
NMT1	P30419	Glycylpeptide N−tetradecanoyltransferase 1	−3.4123	0.0149	−0.9816
BID	P55957	BH3−interacting domain death agonist	−3.2449	0.0159	−0.9313
LRP5	O75197	Low−density lipoprotein receptor−related protein 5	−2.6911	0.0214	0.2322
RCC1L	Q96I51	RCC1−like G exchanging factor−like protein	−2.2961	0.0265	−0.6518
NTHL1	P78549	Endonuclease III−like protein 1	3.0604	0.0172	0.8762
NME6	O75414	Nucleoside diphosphate kinase 6	3.4230	0.0147	0.9849
MTFMT	Q96DP5	Methionyl−tRNA formyltransferase, mitochondrial	3.6846	0.0132	1.0643
MT−ND2	P03891	NADH−ubiquinone oxidoreductase chain 2	3.6882	0.0132	1.0654
COQ10B	Q9H8M1	Coenzyme Q−binding protein COQ10 homolog B, mitochondrial	3.6968	0.0132	1.0680
MRPL12	P52815	39S ribosomal protein L12, mitochondrial	3.9930	0.0120	1.1592
MAFF	Q9ULX9	Transcription factor MafF	4.0860	0.0116	1.7728
VARS	P26640	Valine−−tRNA ligase	4.2708	0.0111	1.2462
KYAT3	Q6YP21	Kynurenine−−oxoglutarate transaminase 3	4.3519	0.0108	1.2720
NDUFB2	O95178	NADH dehydrogenase [ubiquinone] 1 beta subcomplex subunit 2, mitochondrial	4.4299	0.0107	1.2964
DDX28	Q9NUL7	Probable ATP−dependent RNA helicase DDX28	4.6219	0.0102	1.3578
METTL15	A6NJ78	Probable methyltransferase−like protein 15	4.6701	0.0100	1.3733
PFDN2	Q9UHV9	Prefoldin subunit 2	4.6873	0.0100	1.3790
MRPL14	Q6P1L8	39S ribosomal protein L14, mitochondrial	4.7420	0.0098	1.3965
ACAD8	Q9UKU7	Isobutyryl−CoA dehydrogenase, mitochondrial	4.7569	0.0097	1.4013
SMDT1	Q9H4I9	Essential MCU regulator, mitochondrial	4.8376	0.0095	1.4276
SUOX	P51687	Sulfite oxidase, mitochondrial	4.9311	0.0092	1.4582
ATP5E	P56381	ATP synthase subunit epsilon, mitochondrial	4.9648	0.0091	1.4693
IFIT3	O14879	Interferon−induced protein with tetratricopeptide repeats 3	5.0664	0.0088	1.5028

MRPL40	Q9NQ50	39S ribosomal protein L40, mitochondrial	5.1065	0.0088	1.5162
NDUFA12	Q9UI09	NADH dehydrogenase [ubiquinone] 1 alpha subcomplex subunit 12	5.1291	0.0087	1.5237
TYSND1	Q2T9J0	Peroxisomal leader peptide-processing protease	5.1935	0.0086	1.5452
MRPL50	Q8N5N7	39S ribosomal protein L50, mitochondrial	5.2048	0.0086	1.5490
GPD1	P21695	Glycerol-3-phosphate dehydrogenase [NAD(+)], cytoplasmic	5.2342	0.0085	1.5594
GARS	P41250	Glycine--tRNA ligase	5.4844	0.0081	1.6433
GDAP1	Q8TB36	Ganglioside-induced differentiation-associated protein 1	5.4972	0.0081	1.0635
MMAA	Q8IVH4	Methylmalonic aciduria type A protein, mitochondrial	5.5074	0.0081	1.6511
CDK7	P50613	Cyclin-dependent kinase 7	5.5869	0.0075	1.6785
PDP1	Q9P0J1	[Pyruvate dehydrogenase [acetyl-transferring]]-phosphatase 1, mitochondrial	6.0992	0.0067	1.8584
PRDX5	P30044	Peroxiredoxin-5, mitochondrial	6.2022	0.0064	1.8956
ISCU	Q9H1K1	Iron-sulfur cluster assembly enzyme ISCU, mitochondrial	6.2459	0.0064	1.9115
TIMM8A	O60220	Mitochondrial import inner membrane translocase subunit Tim8 A	6.5296	0.0059	2.0163
FDPS	P14324	Farnesyl pyrophosphate synthase	6.5835	0.0059	1.4526
MTERF3	Q96E29	Transcription termination factor 3, mitochondrial	6.5955	0.0059	1.0425
NDUFAF8	A1L188	NADH dehydrogenase [ubiquinone] 1 alpha subcomplex assembly factor 8	6.6567	0.0056	2.0640
COX7C	P15954	Cytochrome c oxidase subunit 7C, mitochondrial	6.9985	0.0052	2.1958
GUK1	Q16774	Guanylate kinase	7.1395	0.0049	2.2518
ARG1	P05089	Arginase-1	7.7613	0.0042	1.9254
ATP5S	Q99766	ATP synthase subunit s, mitochondrial	8.3699	0.0038	2.7830
ENY2	Q9NPA8	Transcription and mRNA export factor ENY2	8.5129	0.0037	2.8501
TFB1M	Q8WVM0	Dimethyladenosine transferase 1, mitochondrial	8.5399	0.0037	2.2804
INPP5B	P32019	Type II inositol 1,4,5-trisphosphate 5-phosphatase	9.6654	0.0026	3.4660
C15orf61	A6NNL5	Uncharacterized protein C15orf61	9.8336	0.0025	3.5666
SLC25A16	P16260	Graves disease carrier protein	10.9029	0.0019	4.3260
TUSC2	O75896	Tumor suppressor candidate 2	11.4897	0.0018	4.2878
C8orf82	Q6P1X6	UPF0598 protein C8orf82	12.1286	0.0016	5.0545
MRPL33	O75394	39S ribosomal protein L33, mitochondrial	12.3575	0.0015	5.9734
GATC	O43716	Glutamyl-tRNA(Gln) amidotransferase subunit C, mitochondrial	12.3778	0.0015	4.4519
LYRM7	Q5U5X0	Complex III assembly factor LYRM7	13.6469	0.0012	10.2875
GCSH	P23434	Glycine cleavage system H protein, mitochondrial	13.6469	0.0012	10.2875
MTFR1	Q15390	Mitochondrial fission regulator 1	13.6469	0.0012	10.2875
RPIA	P49247	Ribose-5-phosphate isomerase	13.6469	0.0012	10.2875
CHCHD5	Q9BSY4	Coiled-coil-helix-coiled-coil-helix domain-containing protein 5	13.6479	0.0012	10.2877
CISD1	Q9NZ45	CDGSH iron-sulfur domain-containing protein 1	13.6479	0.0012	10.2877
MRPL51	Q4U2R6	39S ribosomal protein L51, mitochondrial	13.6479	0.0012	10.2877

IMMP2L	Q96T52	Mitochondrial inner membrane protease subunit 2	13.6479	0.0012	10.2877
MCEE	Q96PE7	Methylmalonyl−CoA epimerase, mitochondrial	13.6479	0.0012	10.2877
ACOX1	Q15067	Peroxisomal acyl−coenzyme A oxidase 1	13.6479	0.0012	10.2877
NOA1	Q8NC60	Nitric oxide−associated protein 1	13.6479	0.0012	10.2877
RAB4B	P61018	Ras−related protein Rab−4B	13.6489	0.0012	10.2880
MRPL36	Q9P0J6	39S ribosomal protein L36, mitochondrial	13.6489	0.0012	10.8727
CYB5B	O43169	Cytochrome b5 type B	13.6499	0.0006	10.2877

Gene name	Accession	Description	TNF_vs_CON_STN	TNF_vs_CON_p−val	log2FC
FSIP2	Q5CZC0	Fibrous sheath−interacting protein 2	−14.6762	0.0010	−10.8727
SLC44A1	Q8WWI5	Choline transporter−like protein 1	−14.6672	0.0010	−10.2877
ACP6	Q9NPH0	Lysophosphatidic acid phosphatase type 6	−11.1272	0.0019	−2.1542
SFXN2	Q96NB2	Sideroflexin−2	−9.3807	0.0031	−2.2534
OMA1	Q96E52	Metalloendopeptidase OMA1, mitochondrial	−8.8599	0.0035	−2.0359
USP48	Q86UV5	Ubiquitin carboxyl−terminal hydrolase 48	−6.4913	0.0061	−0.7826
IFIT3	O14879	Interferon−induced protein with tetratricopeptide repeats 3	−6.4422	0.0062	−1.7558
NOP14	P78316	Nucleolar protein 14	−6.2530	0.0064	−1.6964
COX14	Q96I36	Cytochrome c oxidase assembly protein COX14	−5.6967	0.0079	−1.5266
MAPK14	Q16539	Mitogen−activated protein kinase 14	−4.8422	0.0099	−1.2766
ACAA1	P09110	3−ketoacyl−CoA thiolase, peroxisomal	−4.5852	0.0108	−1.2038
ARMC1	Q9NVT9	Armadillo repeat−containing protein 1	−4.5076	0.0111	−1.1818
NUDT8	Q8WV74	Nucleoside diphosphate−linked moiety X motif 8	−4.4980	0.0111	−1.1791
SARS	P49591	Serine−−tRNA ligase, cytoplasmic	−4.4094	0.0114	−1.1543
TXN	P10599	Thioredoxin	−4.3411	0.0117	−1.1353
DNAJC4	Q9NNZ3	DnaJ homolog subfamily C member 4	−4.3331	0.0117	−1.1330
TYMP	P19971	Thymidine phosphorylase	−4.2409	0.0120	−1.1074
GLT8D1	Q68CQ7	Glycosyltransferase 8 domain−containing protein 1	−4.2153	0.0121	−1.1004
NT5C3A	Q9H0P0	Cytosolic 5'−nucleotidase 3A	−4.0532	0.0128	−1.0555
CTSA	P10619	Lysosomal protective protein	−3.9363	0.0133	−1.0235
TIMM8A	O60220	Mitochondrial import inner membrane translocase subunit Tim8 A	−3.8981	0.0135	−1.0130
TYMS	P04818	Thymidylate synthase	−3.8482	0.0137	−0.9993
C15orf61	A6NNL5	Uncharacterized protein C15orf61	−3.8165	0.0138	−0.9906
PECR	Q9BY49	Peroxisomal trans−2−enoyl−CoA reductase	−3.8086	0.0138	−0.9885
MAP2K2	P36507	Dual specificity mitogen−activated protein kinase kinase 2	−3.7848	0.0140	−0.9820
TAP1	Q03518	Antigen peptide transporter 1	−3.6031	0.0149	−0.9327
PIN4	Q9Y237	Peptidyl−prolyl cis−trans isomerase NIMA−interacting 4	−3.5598	0.0152	−0.9210
NACC2	Q96BF6	Nucleus accumbens−associated protein 2	−3.2507	0.0172	0.7371
PLSCR3	Q9NRY6	Phospholipid scramblase 3	2.5727	0.0238	0.6589
MRS2	Q9HD23	Magnesium transporter MRS2 homolog, mitochondrial	2.7259	0.0220	0.6991

MRPL55	Q7Z7F7	39S ribosomal protein L55, mitochondrial	3.4896	0.0154	0.9022
MRPS18B	Q9Y676	28S ribosomal protein S18b, mitochondrial	3.5283	0.0152	0.9125
POP1	Q99575	Ribonucleases P/MRP protein subunit POP1	3.5959	0.0148	0.9309
REXO2	Q9Y3B8	Oligoribonuclease, mitochondrial	3.7951	0.0138	0.9849
ACAD8	Q9UKU7	Isobutyryl-CoA dehydrogenase, mitochondrial	3.8030	0.0137	0.9870
AK3	Q9UIJ7	GTP:AMP phosphotransferase AK3, mitochondrial	3.8323	0.0136	0.9950
TSPO	P30536	Translocator protein	3.8371	0.0136	0.9964
MRPL24	Q96A35	39S ribosomal protein L24, mitochondrial	3.8466	0.0135	0.9989
FDX1	P10109	Adrenodoxin, mitochondrial	3.9259	0.0133	1.0206
ALDH1B1	P30837	Aldehyde dehydrogenase X, mitochondrial	3.9299	0.0132	1.0217
MRPS24	Q96EL2	28S ribosomal protein S24, mitochondrial	3.9299	0.0132	1.0217
MRPS26	Q9BYN8	28S ribosomal protein S26, mitochondrial	3.9498	0.0131	1.0271
RMDN1	Q96DB5	Regulator of microtubule dynamics protein 1	4.0174	0.0128	1.0457
MTX2	O75431	Metaxin-2	4.0444	0.0128	1.0530
HINT2	Q9BX68	Histidine triad nucleotide-binding protein 2, mitochondrial	4.0867	0.0126	1.0647
MT-ATP6	P00846	ATP synthase subunit a	4.1274	0.0124	1.0761
ATP5H	O75947	ATP synthase subunit d, mitochondrial	4.1410	0.0123	1.0797
MRPL9	Q9BYD2	39S ribosomal protein L9, mitochondrial	4.2073	0.0121	1.0982
SIRT3	Q9NTG7	NAD-dependent protein deacetylase sirtuin-3, mitochondrial	4.2145	0.0121	1.1000
MRPL28	Q13084	39S ribosomal protein L28, mitochondrial	4.2449	0.0120	1.1085
MRPS10	P82664	28S ribosomal protein S10, mitochondrial	4.2609	0.0119	1.1130
CCDC127	Q96BQ5	Coiled-coil domain-containing protein 127	4.2705	0.0119	1.1155
PET100	P0DJ07	Protein PET100 homolog, mitochondrial	4.2905	0.0118	1.1211
BNIP1	Q12981	Vesicle transport protein SEC20	4.3531	0.0115	1.1386
SLC25A46	Q96AG3	Solute carrier family 25 member 46	4.5060	0.0110	1.1814
YWHAH	Q04917	14-3-3 protein eta	4.5197	0.0110	1.1851
PRDX5	P30044	Peroxiredoxin-5, mitochondrial	4.5221	0.0110	1.1859
TIMM21	Q9BVV7	Mitochondrial import inner membrane translocase subunit Tim21	4.5408	0.0109	1.1913
NAXE	Q8NCW5	NAD(P)H-hydrate epimerase	4.6029	0.0106	1.2087
ETFB	P38117	Electron transfer flavoprotein subunit beta	4.6069	0.0106	1.2098
NDUFAF8	A1L188	NADH dehydrogenase [ubiquinone] 1 alpha subcomplex assembly factor 8	4.6676	0.0104	1.2270
AASS	Q9UDR5	Alpha-aminoadipic semialdehyde synthase, mitochondrial	4.8081	0.0099	1.2670
PTRH2	Q9Y3E5	Peptidyl-tRNA hydrolase 2, mitochondrial	4.8341	0.0099	1.2743
MPC2	O95563	Mitochondrial pyruvate carrier 2	4.8748	0.0097	1.2859
PSMA6	P60900	Proteasome subunit alpha type-6	4.8814	0.0097	1.2879
FDX2	Q6P4F2	Ferredoxin-2, mitochondrial	4.8993	0.0096	1.2929
TK2	O00142	Thymidine kinase 2, mitochondrial	5.0081	0.0094	1.3243
PRDX6	P30041	Peroxiredoxin-6	5.0562	0.0092	1.3380
HIBADH	P31937	3-hydroxyisobutyrate dehydrogenase, mitochondrial	5.1218	0.0091	1.3569
PEBP1	P30086	Phosphatidylethanolamine-binding protein 1	5.1449	0.0090	1.3638

L2HGDH	Q9H9P8	L-2-hydroxyglutarate dehydrogenase, mitochondrial	5.1531	0.0090	1.3662
CWC15	Q9P013	Spliceosome-associated protein CWC15 homolog	5.2381	0.0088	1.3910
ACADSB	P45954	Short/branched chain specific acyl-CoA dehydrogenase, mitochondrial	5.2396	0.0088	1.3913
MRPL10	Q7Z7H8	39S ribosomal protein L10, mitochondrial	5.3180	0.0086	1.4143
HSCB	Q8IWL3	Iron-sulfur cluster co-chaperone protein HscB, mitochondrial	5.3218	0.0086	0.8366
DHTKD1	Q96HY7	Probable 2-oxoglutarate dehydrogenase E1 component DHKTD1, mitochondrial	5.3982	0.0085	1.4377
ALDH2	P05091	Aldehyde dehydrogenase, mitochondrial	5.5963	0.0082	1.4965
MTX3	Q5HYI7	Metaxin-3	5.6229	0.0081	1.5043
MRPS7	Q9Y2R9	28S ribosomal protein S7, mitochondrial	5.7764	0.0079	1.5505
TOMM20	Q15388	Mitochondrial import receptor subunit TOM20 homolog	5.8944	0.0077	1.5862
QDPR	P09417	Dihydropteridine reductase	6.0908	0.0073	1.6462
ACSS1	Q9NUB1	Acetyl-coenzyme A synthetase 2-like, mitochondrial	6.1902	0.0068	1.6772
OXCT1	P55809	Succinyl-CoA:3-ketoacid coenzyme A transferase 1, mitochondrial	6.2258	0.0067	1.6881
ECI1	P42126	Enoyl-CoA delta isomerase 1, mitochondrial	6.2316	0.0067	1.6898
SOD2	P04179	Superoxide dismutase [Mn], mitochondrial	6.5287	0.0062	1.7832
FH	P07954	Fumarate hydratase, mitochondrial	6.5663	0.0062	1.7953
DDAH1	O94760	N(G),N(G)-dimethylarginine dimethylaminohydrolase 1	7.0227	0.0056	1.9436
ALDH9A1	P49189	4-trimethylaminobutyraldehyde dehydrogenase	7.2078	0.0054	1.4286
BCS1L	Q9Y276	Mitochondrial chaperone BCS1	7.2669	0.0053	0.4572
NDUFS4	O43181	NADH dehydrogenase [ubiquinone] iron-sulfur protein 4, mitochondrial	7.2728	0.0053	2.0272
SMURF1	Q9HCE7	E3 ubiquitin-protein ligase SMURF1	7.4419	0.0051	1.5085
ECHS1	P30084	Enoyl-CoA hydratase, mitochondrial	7.5156	0.0050	2.1105
NUDT6	P53370	Nucleoside diphosphate-linked moiety X motif 6	7.8312	0.0047	2.2304
NDUFS3	O75489	NADH dehydrogenase [ubiquinone] iron-sulfur protein 3, mitochondrial	7.8805	0.0047	2.2387
NFU1	Q9UMS0	NFU1 iron-sulfur cluster scaffold homolog, mitochondrial	7.9611	0.0045	2.2675
PUS1	Q9Y606	tRNA pseudouridine synthase A, mitochondrial	8.4137	0.0042	0.8712
COA7	Q96BR5	Cytochrome c oxidase assembly factor 7	8.5077	0.0041	2.4710
NUDT9	Q9BW91	ADP-ribose pyrophosphatase, mitochondrial	9.0870	0.0036	2.7010
TXNRD2	Q9NNW7	Thioredoxin reductase 2, mitochondrial	9.4650	0.0032	1.3035
TOMM22	Q9NS69	Mitochondrial import receptor subunit TOM22 homolog	10.2463	0.0027	3.2217
C21orf33	P30042	ES1 protein homolog, mitochondrial	10.4188	0.0027	3.3085
CYB5A	P00167	Cytochrome b5	10.6071	0.0025	1.8588
GADD45GIP1	Q8TAE8	Growth arrest and DNA damage-inducible proteins-interacting protein 1	14.6672	0.0011	10.2877
NDUFA11	Q86Y39	NADH dehydrogenase [ubiquinone] 1 alpha subcomplex subunit 11	14.6762	0.0010	10.8727
COX7C	P15954	Cytochrome c oxidase subunit 7C, mitochondrial	14.6762	0.0010	10.8727
VARS2	Q5ST30	Valine--tRNA ligase, mitochondrial	14.6762	0.0010	10.2877
KIAA0391	O15091	Mitochondrial ribonuclease P protein 3	14.6851	0.0006	10.2877
GUF1	Q8N442	Translation factor GUF1, mitochondrial	14.6851	0.0006	10.2877

Table S2: The MRM method setting for the targeted metabolites. Q1/Q3 transition lists representing 19 unique polar metabolites using both negative and positive ion modes along with CEs, chemical formulas and dwell times.

Ion mode	Precursor Ion Name	Precursor Mz	Precursor Charge	Product Mz	Product Charge	Retention Time	Area	Background	Collision Energy
Negative	L-Aspartate	132.030232	-1	115	-1	1.4	340	1152	5.1
Negative	L-Aspartate	132.030232	-1	88	-1	1.4	1439	1222	5.1
Negative	L-Glutamate	146.045882	-1	128	-1	1.43	47343	962	5.5
Negative	L-Glutamate	146.045882	-1	102	-1	1.43	111319	1046	5.5
Negative	L-Lactate	89.024418	-1	45	-1	2.39	17096	1352	3.8
Negative	L-Lactate	89.024418	-1	43.02	-1	2.39	172218	1285	3.8
Negative	D-Fructose 6-phosphate	259.022443	-1	79	-1	3.93	5384	5262	9
Negative	D-Glucose 6-phosphate	259.022443	-1	199	-1	1.41	2096	6423	9
Negative	alpha-D-Ribose 5-phosphate	229.011878	-1	97	-1	1.4	5618	9038	8.1
Negative	alpha-D-Ribose 5-phosphate	229.011878	-1	79	-1	1.87	8575	9044	8.1
Negative	Succinate	117.019333	-1	99	-1	4.11	1595	1183	4.6
Negative	Succinate	117.019333	-1	73	-1	4.09	17762	1176	4.6
Negative	L-Malate	133.014247	-1	115	-1	1.95	31100	1492	5.1
Negative	Fumarate	115.003683	-1	71	-1	3.38	976	1170	4.6
Negative	Oxaloacetate	130.998597	-1	87	-1	1.2	6673	706	5.1
Negative	cis-Aconitate	173.009162	-1	85	-1	3.54	878	5174	6.4
Negative	Citrate	191.019727	-1	111	-1	3.13	98486	10187	6.9
Negative	Citrate	191.019727	-1	87	-1	3.13	30769	4659	6.9
Negative	D-Fructose 1, 6-bisphosphate	338.988774	-1	241	-1	2.43	1489	7652	11.5
Negative	D-Fructose 1, 6-bisphosphate	338.988774	-1	79	-1	1.41	5900	7667	11.5
Positive	L-Glutamate	148.060434	1	84.1	1	1.43	769403	1948	5.6
Positive	L-Aspartate	134.044784	1	74	1	2.57	83727	2328	5.2
Negative	Dihydroxyacetone phosphate	168.990749	-1	97.03	-1	1.41	595	11050	6.2
Negative	Dihydroxyacetone phosphate	168.990749	-1	79	-1	1.41	1679	11484	6.2
Negative	Pyruvate	87.008768	-1	43.02	-1	1.82	304	1963	3.7
Negative	D-Glucose 6-phosphate	259.022443	-1	198.98	-1	1.4	2151	4732	9
Negative	Dihydroxyacetone phosphate	168.990749	-1	79	-1	1.41	1679	11484	6.2
Negative	Fumarate	115.003683	-1	71.01	-1	3.35	990	968	4.6
Negative	Isocitrate	191.019727	-1	117	-1	2	208	1043	6.9
Negative	Isocitrate	191.019727	-1	73	-1	1.96	524	1055	6.9

Reference

1. Padoan,A., Plebani, M. &Basso, D. Inflammation and Pancreatic Cancer: Focus on Metabolism, Cytokines, and Immunity. Int J Mol Sci 20, doi:10.3390/ijms20030676(2019).

2. Qu,X., Tang, Y. &Hua, S. Immunological Approaches Towards Cancer and Inflammation: A Cross Talk. Front Immunol 9, 563, doi:10.3389/fimmu.2018.00563(2018).

3. Pullamsetti,S. S. et al. Lung cancer-associated pulmonary hypertension: Role of microenvironmental inflammation based on tumor cell-immune cell cross-talk. SciTransl Med 9, doi:10.1126/scitranslmed.aai9048 (2017).

4. Wang,F., Meng, W., Wang, B. &Qiao, L. Helicobacter pylori-induced gastric inflammation and gastric cancer. Cancer Lett 345, 196-202, doi:10.1016/j.canlet.2013.08.016(2014).

5. Pierce,B. L. et al. Elevated biomarkers of inflammation are associated with reduced survival among breast cancer patients. J Clin Oncol 27, 3437-3444, doi:10.1200/JCO.2008.18.9068 (2009).

6. Bachelot,T. et al. Prognostic value of serum levels of interleukin 6 and of serum and plasma levels of vascular endothelial growth factor in hormone-refractorymetastatic breast cancer patients. Br J Cancer 88, 1721-1726, doi:10.1038/sj.bjc.6600956 (2003).

7. Hanahan, D. &Weinberg, R. A. Hallmarks ofcancer: the next

generation. Cell 144, 646-674, doi:10.1016/j.cell.2011.02.013(2011).

8. Cai,X. et al. Inflammatory factor TNF-alpha promotes the growth of breast cancervia the positive feedback loop of TNFR1/NF-kappaB (and/orp38)/p-STAT3/HBXIP/TNFR1. Oncotarget 8, 58338-58352, doi:10.18632/oncotarget.16873 (2017).

9. Yu,M. et al. Targeting transmembrane TNF-alpha suppresses breast cancer growth. Cancer Res 73, 4061-4074, doi:10.1158/0008-5472.CAN-12-3946 (2013).

10. Ma,Y. et al. IL-6, IL-8 and TNF-alpha levels correlate with disease stage in breast cancer patients. Adv Clin Exp Med 26, 421-426, doi:10.17219/acem/62120(2017).

11. Hussain,S. P., Hofseth, L. J. &Harris, C. C. Radical causes of cancer. Nat Rev Cancer 3, 276-285, doi:10.1038/nrc1046 (2003).

12. Ham,B., Fernandez, M. C., D'Costa, Z. &Brodt, P. The diverse roles of the TNFaxis in cancer progression and metastasis. Trends Cancer Res 11, 1-27 (2016).

13. Maolake,A. et al. Tumor necrosis factor-alpha induces prostate cancer cell migration in lymphatic metastasis through CCR7 upregulation. Cancer Sci 109, 1524-1531, doi:10.1111/cas.13586 (2018).

14. Singh,K. et al. NLRX1 acts as tumor suppressor by regulating TNF-alpha induced apoptosis and metabolism in cancer cells. Biochim Biophys Acta 1853, 1073-1086,doi:10.1016/j.bbamcr.2015.01.016 (2015).

15. Mishra,P. &Chan, D. C. Metabolic regulation of mitochondrial dynamics. J CellBiol 212, 379-387, doi:10.1083/jcb.201511036 (2016).

16. Sandhir,R., Halder, A. &Sunkaria, A. Mitochondria as a centrally positioned hub inthe innate immune response. Biochim Biophys Acta Mol Basis Dis 1863, 1090-1097, doi:10.1016/j.bbadis.2016.10.020 (2017).

17. Vyas,S., Zaganjor, E. &Haigis, M. C. Mitochondria and Cancer. Cell 166,555-566, doi:10.1016/j.cell.2016.07.002 (2016).

18. Lavie,J. et al. Ubiquitin-Dependent Degradation of Mitochondrial Proteins Regulates Energy Metabolism. Cell Rep 23, 2852-2863, doi:10.1016/j.celrep.2018.05.013(2018).

19. Rosenfeld,J., Capdevielle, J., Guillemot, J. C. &Ferrara, P. In-gel digestion of proteins for internal sequence analysis after one- or two-dimensional gel electrophoresis. Anal Biochem 203, 173-179, doi:10.1016/0003-2697(92)90061-b(1992).

20. Pavelka,N. et al. Statistical similarities between transcriptomics and quantitative shotgun proteomics data. Mol Cell Proteomics 7, 631-644, doi:10.1074/mcp.M700240-MCP200 (2008).

21. Team,R. D. C. R: A Language and Environment for Statistical Computing (R Foundation for Statistical Computing, 2009)

22. Thomas,L., Stefanski, L. &Davidian, M. A moment-adjusted imputation method for measurement error models. Biometrics 67, 1461-1470,

doi:10.1111/j.1541-0420.2011.01569.x(2011).

23. Thomas,P. D. et al. PANTHER: a library of protein families and subfamilies indexed by function. Genome Res 13, 2129-2141, doi:10.1101/gr.772403 (2003).

24. Wittig,I., Braun, H. P. & Schagger, H. Blue native PAGE. Nat Protoc 1, 418-428, doi:10.1038/nprot.2006.62 (2006).

25. MacLean,B. et al. Skyline: an open source document editor for creating and analyzing targeted proteomics experiments. Bioinformatics 26, 966-968, doi:10.1093/bioinformatics/btq054 (2010).

26. Anaya,J. OncoLnc: linking TCGA survival data to mRNAs, miRNAs, andlncRNAs. PeerJ Comput. Sci. 2, e67 (2016).

27. Li,B. et al. Comprehensive analyses of tumor immunity: implications for cancer immunotherapy. Genome Biol 17, 174, doi:10.1186/s13059-016-1028-7 (2016).

28. Ricci,J.-E. et al. Disruption of Mitochondrial Function during Apoptosis Is Mediatedby Caspase Cleavage of the p75 Subunit of Complex I of the Electron TransportChain. Cell 117, 773-786, doi:https://doi.org/10.1016/j.cell.2004.05.008(2004).

29. H□ttemann,M. et al. Regulation of mitochondrial respiration and apoptosis through cel lsignaling: Cytochrome c oxidase and cytochrome c in ischemia/reperfusion injuryand inflammation. Biochimica et Biophysica Acta (BBA) - Bioenergetics 1817,598-609, doi:https://doi.org/10.1016/j.bbabio.2011.07.001 (2012).

30. Li,B. et al. Comprehensive analyses of tumor immunity:

implications for cancer immunotherapy. Genome Biol 17, 174, doi:10.1186/s13059-016-1028-7 (2016).

31. Ans□,E. et al. The mitochondrial respiratory chain is essential for haematopoieticstem cell function. Nature Cell Biology 19, 614, doi:10.1038/ncb3529 (2017).

32. S□nchez,E. et al. LYRM7/MZM1L is a UQCRFS1 chaperone involved in the last steps of mitochondrial Complex III assembly in human cells. Biochimica et Biophysica Acta (BBA) - Bioenergetics 1827, 285-293, doi:https://doi.org/10.1016/j.bbabio.2012.11.003 (2013).

33. Cruciat,C. M., Hell, K., F□lsch, H., Neupert, W. &Stuart, R. A. Bcs1p, an AAA-family member, is a chaperone for the assembly of the cytochrome bc(1)complex. EMBO J 18, 5226-5233, doi:10.1093/emboj/18.19.5226 (1999).

34. Kim,H. C., Chang, J., Lee, H. S. &Kwon, H. J. Mitochondrial UQCRB as a new molecular prognostic biomarker of human colorectal cancer. Exp Mol Med 49,e391, doi:10.1038/emm.2017.152 (2017).

35. Barel,O. et al. Mitochondrial complex III deficiency associated with a homozygousmutation in UQCRQ. Am J Hum Genet 82, 1211-1216, doi:10.1016/j.ajhg.2008.03.020(2008).

36. Jerby,L. et al. Metabolic associations of reduced proliferation and oxidative stress in advanced breast cancer. Cancer Res 72, 5712-5720, doi:10.1158/0008-5472.CAN-12-2215(2012).

37. Kung,H.-N., Marks, J. R. &Chi, J.-T. Glutamine synthetase is a genetic determinant of cell type-specific glutamine

independence in breast epithelia.PLoS Genet 7, e1002229-e1002229, doi:10.1371/journal.pgen.1002229 (2011).

38. Pozniak,Y. et al. System-wide Clinical Proteomics of Breast Cancer Reveals Global Remodeling of Tissue Homeostasis. Cell Systems 2, 172-184, doi:https://doi.org/10.1016/j.cels.2016.02.001 (2016).

39. Pustylnikov,S., Costabile, F., Beghi, S. &Facciabene, A. Targeting mitochondria in cancer: current concepts and immunotherapy approaches. Transl Res 202, 35-51, doi:10.1016/j.trsl.2018.07.013 (2018).

40. Allinen,M. et al. Molecular characterization of the tumor microenvironment in breast cancer. Cancer Cell 6, 17-32, doi:10.1016/j.ccr.2004.06.010 (2004).

41. Shenoi,M. M. et al. Nanoparticle delivered vascular disrupting agents (VDAs): use ofTNF-alpha conjugated gold nanoparticles for multimodal cancer therapy. Mol Pharm 10, 1683-1694, doi:10.1021/mp300505w (2013).

42. Dondossola,E. et al. Self-targeting of TNF-releasing cancer cells in preclinical models of primary and metastatic tumors. Proc Natl Acad Sci U S A 113, 2223-2228, doi:10.1073/pnas.1525697113 (2016).

43. Wu,T. H. et al. Long-term suppression of tumor growth by TNF requires a Stat1- and IFN regulatory factor 1-dependent IFN-gamma pathway but not IL-12 or IL-18. JImmunol 172, 3243-3251, doi:10.4049/jimmunol.172.5.3243 (2004).

44. Sazanov,L. A. &Hinchliffe, P. Structure of the hydrophilic domain of respiratory complex I from Thermus thermophilus. Science 311, 1430-1436, doi:10.1126/science.1123809 (2006).

45. Mathiesen,C. &Hagerhall, C. Transmembrane topology of the NuoL, M and N subunits of NADH:quinone oxidoreductase and their homologues among membrane-bound hydrogenases and bona fide antiporters. Biochim Biophys Acta 1556, 121-132, doi:10.1016/s0005-2728(02)00343-2 (2002).

46. Stroud,D. A. et al. Accessory subunits are integral for assembly and function of human mitochondrial complex I. Nature 538, 123, doi:10.1038/nature19754 (2016).

47. Tretter,L., Patocs, A. & Chinopoulos, C. Succinate, an intermediate in metabolism, signal transduction, ROS, hypoxia, and tumorigenesis. Biochim Biophys Acta 1857, 1086-1101, doi:10.1016/j.bbabio.2016.03.012 (2016).

48. Laukka,T. et al. Fumarate and Succinate Regulate Expression of Hypoxia-inducible Genesvia TET Enzymes. J Biol Chem 291, 4256-4265, doi:10.1074/jbc.M115.688762(2016).

49. Putignani,L. et al. Preliminary evidences on mitochondrial injury and impaired oxidative metabolism in breast cancer. Mitochondrion 12, 363-369, doi:10.1016/j.mito.2012.02.003 (2012).

50. Selak,M. A. et al. Succinate links TCA cycle dysfunction to oncogenesis by inhibiting HIF-alpha prolyl hydroxylase. Cancer Cell 7, 77-85, doi:10.1016/j.ccr.2004.11.022 (2005).

51. Yang,M., Soga, T. &Pollard, P. J. Oncometabolites: linking

altered metabolism with cancer. J Clin Invest 123, 3652-3658, doi:10.1172/JCI67228 (2013).

52. Sullivan,L. B. et al. Supporting Aspartate Biosynthesis Is an Essential Function of Respiration in Proliferating Cells. Cell 162, 552-563, doi:10.1016/j.cell.2015.07.017 (2015).

53. Birsoy,K. et al. An Essential Role of the Mitochondrial Electron Transport Chain inCell Proliferation Is to Enable Aspartate Synthesis. Cell 162, 540-551, doi:10.1016/j.cell.2015.07.016 (2015).

54. Maio,N. et al. Cochaperone binding to LYR motifs confers specificity of iron sulfur cluster delivery. Cell Metab 19, 445-457, doi:10.1016/j.cmet.2014.01.015(2014).

55. Jerby,L. et al. Metabolic associations of reduced proliferation and oxidative stress in advanced breast cancer. Cancer Res 72, 5712-5720, doi:10.1158/0008-5472.CAN-12-2215 (2012).

56. Sullivan,L. B. et al. Supporting Aspartate Biosynthesis Is an Essential Function of Respiration in Proliferating Cells. Cell 162, 552-563, doi:10.1016/j.cell.2015.07.017 (2015).

57. Lehninger, A L. et al. Mitochondria and calcium ion transport.The Biochemical journal119,2, 129-38. doi:10.1042/bj1190129 (1970).

58. Schon EA, Dencher NA. Heavy breathing: energy conversion by mitochondrial respiratory supercomplexes.Cell Metab 9, 1-3, (2009).

국문 초록

그동안 암세포 특이적인 대사 기전으로 와버그 효과(Warburg effect)가 가장 큰 가설로 자리 잡고 있었다. 그러나 최근 암세포의 종류별 대사 기전이 다를 수 있으며, 병기별 대사에 리프로그래밍(reprogramming)이 일어난 다는 사실이 밝혀졌고, 이에 암의 이종성(heterogeneity)에 따른 대사의 차이를 이해하고 규명하려는 연구가 계속되어 왔다. 대사의 중심에 있는 미토콘드리아는 암의 형성과 생존에 필요한 에너지와 구성 요소(building block)를 생성하고 산화/환원을 조절하며, 전이에도 연관이 있다고 밝혀졌다. 암의 초기 단계에서 발현량이 높아지는 사이토카인인 종양괴사인자(TNF-α)는 전염증성 미세환경의 생성을 돕고, 암세포의 전이를 유도한다고 알려졌다. 그러나 TNF-α가 암세포의 종류에 따라 어떠한 대사의 변화를 유도하는지, 그리고 항종양성(anti-tumor)과 항세포죽음(anti-apoptosis)의 두 가지 기전 중 어느 것을 유도하는지에 대한 내용은 아직 규명되지 않았다. 본 연구에서는 ER/PR 양성 세포인 MCF7과 ER/PR 음성 세포인 MDA-MB231, 두 가지의 유방암 세포주를 이용하여, TNF-α로 인해 대사가 어떻게 리프로그래밍되는지 그의 기전을 질량분석기를 이용한 단백체와 대사체의 분석으로 규명하고자 했다. 분석 결과, TNF-α에 의한 대사 리프로그래밍은 두 세포주에서 다르게 유도되었고, 미토콘드리아 대사에서 중요한 역할을 하는 전자전달계(ETC) 컴플랙스의 응집과 활성에 변화를 관찰할 수 있었다. ETC 응집의 형성을 저해하는 단백질 마커를 찾고자 본 연구진은 단백질의 국소화와 변성에 관여하는 유비퀴틴화의 활성 변화를 관찰했고, 대사 적응을 방해하여 암 치료에 사용될 수 있는 후보 마커를 발굴했다.

주요어 :
단백체학, 대사체학, 유방암 이질성, 종양괴사인자, 미토콘드리아
학 번 : 2018-26193